universität wien

MASTERARBEIT / MASTER'S THESIS

Titel der Masterarbeit / Title of the Master's Thesis

„JAK1/2 Signaling in KRAS mutated Lung Adenocarcinoma“

verfasst von / submitted by

Maša Bereš, BSc

angestrebter akademischer Grad / in partial fulfilment of the requirements for the degree of

Master of Science (MSc)

Wien, 2024 / Vienna, 2024

Studienkennzahl lt. Studienblatt / degree programme code as it appears on the student record sheet:	UA 066 606
Studienrichtung lt. Studienblatt / degree programme as it appears on the student record sheet:	Master Drug Discovery and Development
Betreut von / Supervisor:	Univ. - Prof. Dr. Emilio Casanova

Acknowledgments

First, I would like to express my gratitude to Prof. Dr. Emilio Casanova for giving me the opportunity to work in his laboratory. Next, I would like to thank Dr. Herwig Moll for his support and guidance throughout this project. Special thanks to my colleagues Christoph, Monika, Corina, Sarah and especially Seungyeon whose input and suggestions were very helpful and greatly appreciated making this journey unforgettable.

I would also like to thank my parents for their continuous support and encouragement every step of the way, from the start of my studies to this day. Last, but certainly not least, I would like to thank my partner, Tarik, for not being only my moral support, but also for joining me in the lab on weekends and showing off his impressive pipetting skills. And during those intense thesis- writing sessions in the library, his thoughtful gesture of bringing me coffee and sweets made those short breaks even sweeter.

Thank you!

Abstract

Lung cancer is the leading cause of cancer deaths worldwide. The tumorigenesis of KRAS-mutated lung adenocarcinoma (LUAD) is associated with an inflammatory process. Accordingly, Janus kinases (JAK) as core molecules in inflammatory events, present an attractive therapeutic targets.

To assess the role of JAKs in T-cell dependent experimental model, we took advantage of KPO cell line, which in addition to $KRAS^{G12D}$ driver mutation and p53 deletion also expresses highly immunogenic ovalbumin transgene, and thus closely resembles human neoantigens. Systemic JAK1/2 inhibition with ruxolitinib, however, facilitated growth of subcutaneous tumors in immunocompetent C57BL6/N mice. Decreased tumor infiltration of immune cells suggests that ruxolitinib primarily impacted immune cells in immunosuppressive manner, rather than tumor cells. To further investigate role of JAKs in tumor cells, single JAK1 and JAK2 as well as double JAK1/2 knockouts (KOs) were created using CRISPR/Cas9. Targeting JAK1 or JAK2 alone or in combination abrogated IFN-γ mediated signaling resulting as demonstrated by reduced MHC-I and PD-L1 expression levels. While intrinsic JAK1/2 deletion did not slow the growth of subcutaneous tumors, orthotopic transplantation led to significantly decreased survival of recipients of JAK2 KO cells, but not JAK1 KO or JAK1/2 expressing controls. This raises the importance of the tumor microenvironment influencing lung tumorigenesis.

Overall, our results suggest that combining systemic JAK1/2 inhibition with standard therapy for KRAS-driven LUAD, immunotherapy, does not confer beneficial effect on tumorigenesis. However, further studies should focus on elucidating tumor intrinsic role of JAK2, with the potential of identifying novel therapeutic targets.

Zusammenfassung

Lungenkrebs ist weltweit die häufigste Todesursache bei Krebserkrankungen. Die Tumorgenese des KRAS-mutierten Lungenadenokarzinoms ist mit einem entzündlichen Prozess verbunden. Dementsprechend stellen Januskinasen (JAK) als Kernmoleküle bei entzündlichen Ereignissen attraktive therapeutische Ziele dar.

Um die Rolle von JAKs in einem T-Zell-abhängigen experimentellen Modell zu bewerten, nutzen wir die KPO-Zelllinie, die neben der $KRAS^{G12D}$-Treibermutation und der p53-Deletion auch das hochimmunogene Ovalbumin-Transgen exprimiert und somit menschlichen Neoantigenen ähnelt. Die systemische JAK1/2 Inhibition mit Ruxolitinib begünstigte jedoch das Wachstum subkutaner Tumore bei immunokompetenten C57BL6/N-Mäusen. Die verringerte Tumorinfiltration von Immunzellen legt nahe, dass Ruxolitinib hauptsächlich Immunzellen auf immunosuppressive Weise beeinflusste, anstatt Tumorzellen. Um die Rolle von JAKs weiter zu untersuchen, wurden JAK1 und JAK2, sowie doppelte JAK1/2 Knockouts mit Hilfe von CRISPR/Cas9 erstellt. Die Ausrichtung auf JAK1 oder JAK2 allein oder in Kombination hob die, durch reduzierte MHC-I und PD-L1 Expressionsniveaus, nachgewiesene IFN-γ vermittelte Signalübertragung auf. Während die intrinsische JAK1/2 Deletion das Wachstum subkutaner Tumore nicht verlangsamte, führte die orthotope Transplantation zu einer signifikant verringerten Überlebensrate bei Empfängern von JAK2-Knockout Zellen, jedoch nicht bei JAK1-KO oder JAK1/2 exprimierenden Kontrollen. Dies unterschreibt die Bedeutung des Tumormikromilleus für die Lungen-Tumorgenese.

Insgesamt legen unsere Ergebnisse nahe, dass die Kombination einer systemischen JAK1/2 Inhibition mit der Standardtherapie für KRAS-getriebene Lungenadenokarzinome, der Immuntherapie, keinen günstigen Effekt auf die Tumorgenese hat. Weitere Studien sollten sich jedoch darauf konzentrieren, die intrinsische Tumorrolle von JAK2 zu erläutern, mit dem Potenzial, neuartige therapeutische Ziele zu identifizieren.

List of abbreviations

ALK - Anaplastic lymphoma kinase

BAL - Bronchoalveolar lavage

BRAF - V-raf murine sarcoma viral oncogene homolog B

EGFR - Epidermal growth factor receptor

GAP - GTPase activating protein

GDP - Guanosine diphosphate

GEF - Guanine nucleotide exchange factor

GTP - Guanosine triphosphate

HER2 - Human epidermal growth factor receptor 2

IFN - Interferon

IL - Interleukin

JAK - Janus kinase

JAKi - Janus kinase inhibitor

KO - Knockout

KRAS - Kirsten rat sarcoma viral oncogene

LDCT - Low- dose computed tomography

LUAD - Lung adenocarcinoma

MHC - Major histocompatibility complex

MPN - Myeloproliferative neoplasms

Nf-kB - Nuclear factor kappa B

NK cells - Natural killer cells

NSCLC - Non-small cell lung cancer

OVA - Ovalbumin

PBS - Phosphate buffered saline

PD-L1 - Programmed cell death ligand 1

PMFS - Phenylmethanesulfonyl fluoride solution

ROS I - c-ROS oncogene I

SLCL - Small cell lung cancer

STAT - Signal transducer and activator of transcription

TME - Tumor microenvironment

TKI - Tyrosine kinase inhibitors

Key terms

Inflammation

JAK/STAT signaling pathway

KRAS

Lung adenocarcinoma

Ovalbumin

Ruxolitinib

Table of Content

1. INTRODUCTION

1.1. Cancer

Cancer is the leading cause of deaths globally (Bray et al., 2021). According to the GLOBOCAN 2020 database, there is an estimation of 19.3 million new cancer cases, which accounts for 9.9 million cancer deaths worldwide. Most commonly diagnosed type of cancer is female breast cancer followed by lung and colorectal cancer (Sung et al., 2021). However, lung cancer remains the deadliest malignancy globally with a 5-year survival rate of 13% in Europe (Sant et al., 2023).

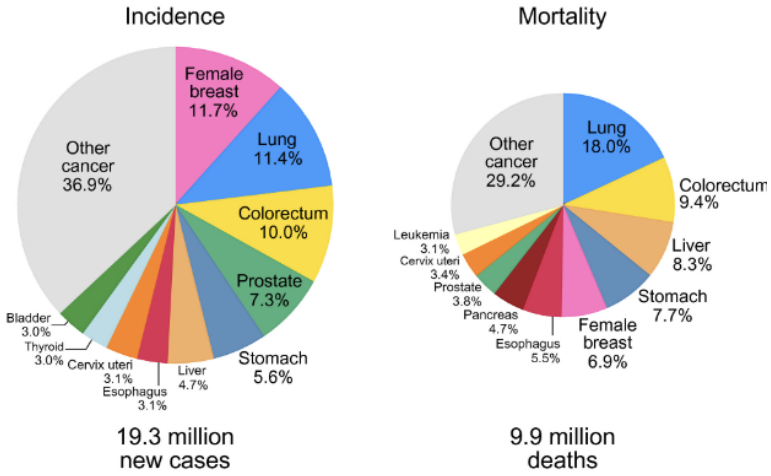

Figure 1: Incidence and mortality of most commonly diagnosed cancers in both sexes (Sung et al., 2021)

1.2. Types of Lung Cancer

Most common type of lung cancer is non-small cell lung cancer (NSCLC), which accounts for 85% of all lung cancer cases, and the remaining 15% is classified as small cell lung cancer (SCLC). Despite the diverse histological patterns observed in NSCLC, most tumors can be categorized into three main groups including squamous cell carcinoma, adenocarcinomas and large cell carcinomas. Most abundant form of NSCLC are adenocarcinomas arising from mucosal glands and accounting for 40% of all NSCLC cases (Wistuba et al., 2018).

1.3. Diagnosis

Poor survival rates in lung cancer usually result from diagnoses made at an already advanced stages of disease (Babar, Raj and Anjum, 2020). Presently, chest x-ray or a low-dose computed tomograpgy (LDCT) scans are used routinely for lung cancer screening. Cancer diagnosis is usually confirmed through tissue biopsy, which can be conducted using methods such as bronchoscopy, CT-guided needle biopsy, as well as non-invasive liquid biopsy (Nooreldeen and Bach, 2021). Depending on the type of lung cancer, molecular testing is performed to detect specific genetic mutations, which guide treatment decisions (Shim et al., 2017). Additionally, staging plays a crucial role as it predicts prognosis and dictates treatment modalities. For staging purposes, TNM system is applied which characterizes tumors based on the size and extent of primary tumor (T), involvement of the lymph nodes (N) and presence of metastasis (Koukis et al., 2013).

1.4. Risk factors

Lung, as an open organ where gas exchange occurs, is easily affected by many pathogens, pollutants, oxidants, gases and poisons inhaled from the air. Extended periods of exposure to inhalable silica dust, mineral fibers, air particulate matter and smoke have the potential to trigger development of lung cancer (Tan et al., 2021). Predominant factor contributing to most lung cancers is persistent exposure to tobacco smoke (Gandini et al., 2007). Carcinogens found in tobacco smoke increase oxidative stress of tissue causing inflammation, which in turn increases likelihood of lung cancer (Gomes et al., 2014). Moreover, previous lung diseases, including tuberculosis, pneumonia, emphysema and chronic bronchitis also influence lung cancer risk independently of tobacco use (Brenner et al., 2012). In addition to environmental exposure, multiple genetic and epigenetic aberrations are involved in the development of lung cancer (Molina et al., 2008).

1.5. Oncogenic Drivers in NSCLC

Oncogenic driver mutations are known to lead to constitutive activation of signaling pathways responsible for cell growth and proliferation. Several oncogenic driver mutations have been identified in NSCLC including genes encoding for epidermal growth factor receptor (EGFR), Kirsten rat sarcoma viral oncogene (KRAS), anaplastic lymphoma kinase (ALK), c-ROS oncogene I (ROS I), v-raf murine sarcoma viral oncogene homolog B (BRAF), human epidermal growth factor 2 (HER2), etc. (Zhou et al., 2013). Among these, KRAS genes

represent the most frequent human oncogenes accounting for 20-25% of NSCLC cases, almost exclusively detected in adenocarcinomas (Friedlaender et al., 2020). Second most common driver in NSCLC is EGFR, usually occurring in non-smokers. While standard treatment for patients with activating EGFR mutations includes tyrosine kinase inhibitors (TKIs), which extend progression free survival beyond cytotoxic therapies, development of targeted therapy for KRAS was less successful (Passaro et al., 2021).

1.6. KRAS

KRAS is one of the three RAS protein isoforms, other two including HRAS and NRAS. It is the most frequently mutated isoform in human cancers. RAS proteins, members of the guanosine triphosphatases (GTPases), function as intracellular guanine nucleotide binding proteins (G proteins) crucial for cell growth regulation, differentiation and apoptosis. They act as a molecular switch and alternate between active and inactive form based on the presence or absence of GTP molecule. RAS-GTP complex, activated by guanine nucleotide exchange factors (GEFs), acts on downstream signaling effectors including Raf-MEK-ERK and PI3K-AKT-mTOR ultimately promoting cell growth and survival (Figure 2). On the other hand, RAS signaling is terminated by the action of GTPase activating proteins (GAPs) which favor GTP to GDP hydrolysis (Román et al., 2018; Velcich et al., 2006; Zhu et al., 2021).

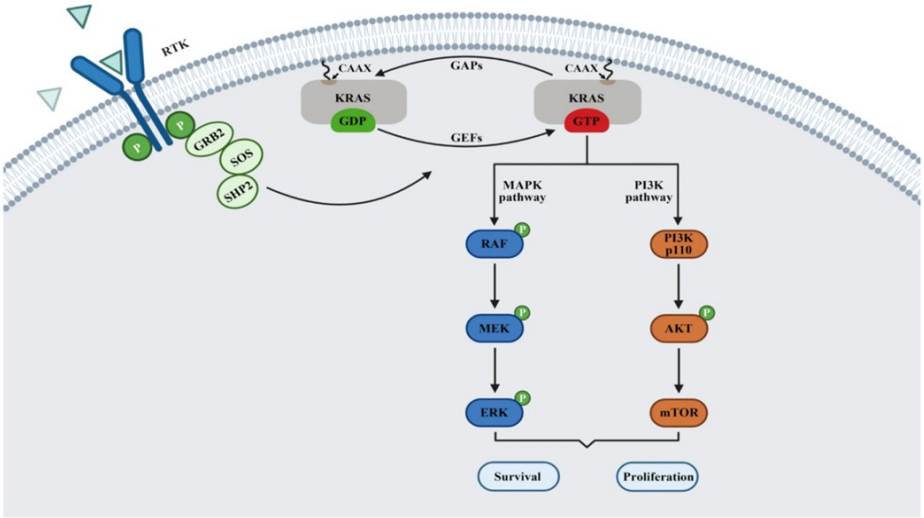

Figure 2: **KRAS signaling**. Upon receptor tyrosine kinase stimulation, guanine nucleotide exchange factor SOS in association with GRB2 and SPH2 activates KRAS by promoting GTP binding. In GTP-bound form, KRAS acts on downstream effectors promoting cell survival and proliferation. GAPs promote GTP to GDP hydrolysis leading to KRAS inactivation. (Adapted from Zhu et al., 2021).

Oncogenic KRAS mutations prevent GTP hydrolysis leading to the accumulation of active form of KRAS and constitutive activation of KRAS signaling. Most common mutations occur in

codon 12 or 13 with G12D mutation as the most prevalent one, followed by G12V and G12C. In KRAS mutated LUAD, G12C is the most frequent one (Zeissig et al., 2023).

1.7. Treatment options for KRAS-mutated LUAD

For a long period of time, KRAS was considered challenging pharmacological target due to the absence of drug binding pockets as well as its smooth and shallow surface. KRAS mutant lung cancer is closely linked to an immune-evasive phenotype and its signaling is believed to be involved in shaping such immunosuppressive environment (Mugarza et al., 2022). Studies indicate that KRAS mutant tumors, strongly associated with cigarette smoking, are more likely to exhibit PD-L1 expression in patients with history of smoking (Ahrendt et al., 2001; Calles et al., 2015). Thus, standard front-line treatment for KRAS-mutated NSCLC follows that of non-oncogene driven NSCLC including immunotherapy together with chemotherapy (Chevallier et al., 2021). Overall, chemotherapy was associated with poor prognosis (Marabese et al., 2015; Mellema et al., 2013). Even though immunotherapy seems to be more effective choice than chemotherapy, patients with KRAS mutations usually have a poor response to current standard treatments, indicating the need for targeted therapy (Amanam et al., 2020).
Presently, sotorasib and adagrasib have gained clinical approval as a small molecule inhibitors for treating patients with previously treated KRAS G12C mutant NSCLC. They bind covalently and irreversibly to mutant KRAS G12C in NSCLC cells and inhibit downstream signaling effects that promote cancer cell proliferation (Mausey and Halford, 2023). In contrast, there are no clinically approved inhibitors for other mutations. Second-line treatment with sotorasib has shown to be beneficial compared to chemotherapy with significant increase in progression-free survival and 34% decrease in the relative risk of disease progression or mortality (de Langen et al., 2023). However, as for any other small molecule inhibitor, resistance may emerge over time in response to targeted therapies (Ryan et al., 2019). Considering that less than 50% of patients initially respond to sotorasib or adagrasib, one can assume that some patients already present intrinsic resistance to G12C inhibition (Chevallier et al., 2021). Therefore, there is an urgent need to identify novel targets for KRAS-mutated LUAD by either interfering with KRAS downstream effectors or other key signaling pathways involved in tumorigenesis.

1.8. KRAS and tumor-promoting inflammation

One of the important characteristics of malignant tumors is the persistence of chronic inflammation. Clinical and epidemiological studies have shown strong association between inflammation, inflammatory microenvironment and lung cancer (Tan et al., 2021). It has been observed that inflammation determines the cell fate of multiple components of the complex

tumor microenvironment (TME), and thus creates a tumor supporting niche and effectively shapes the host response. In addition, standard therapies such as chemotherapy and irradiation may elicit inflammatory response and further impact TME (Denk and Greten, 2022). Stromal and immune cells within TME communicate either directly or via chemokines and cytokines production to control tumor growth. The concept of tumor-promoting inflammation has been tightly associated with KRAS mutations highlighting their importance in tumorigenesis (Pereira et al., 2022). Its ability to induce nuclear factor (NF)-kB activation in fibroblasts and epithelial cells provided the first evidence of its potential to drive proinflammatory signaling in transformed cells (Cullis, Das and Bar-Sagi, 2017).

Oncogenic KRAS induces expression of several proinflammatory cytokines, chemokines and signaling pathways known to lead to tumor promotion and invasiveness (Hamarsheh et al., 2020). For instance, cytokine interleukin 6 (IL6), has been suggested to play a central role in linking inflammation and cancer with oncogenic KRAS inducing its secretion in different cell types (Hamarsheh et al., 2020). IL6 signaling, mediated through activation of Janus kinase (JAK) and leading to subsequent phosphorylation of transducer and activator of transcription 3 (STAT3), is one of the important inflammatory signaling pathways involved in many physiological as well as pathological processes (Huang, Lang and Li, 2022). As it has been demonstrated by Brooks et al., signaling pathways activated by IL6 promote KRAS-driven lung tumorigenesis.

Other inflammatory cytokines secreted by immune, stromal and tumor cells, such as CCL5, via nuclear factor (NF)-kB, facilitate the activation of JAK/STAT signaling pathway (Karim et al., 2022; Denk and Greten, 2022). Also, secretion of CCL5 in oncogenic KRAS expressing cells is enhanced by IL6 signaling circuit (Golay and Barbie, 2014). Given the important role of JAK activation in tumor-promoting inflammation and tumorigenesis, targeting JAKs emerges as a possible strategy for KRAS mutated LUAD.

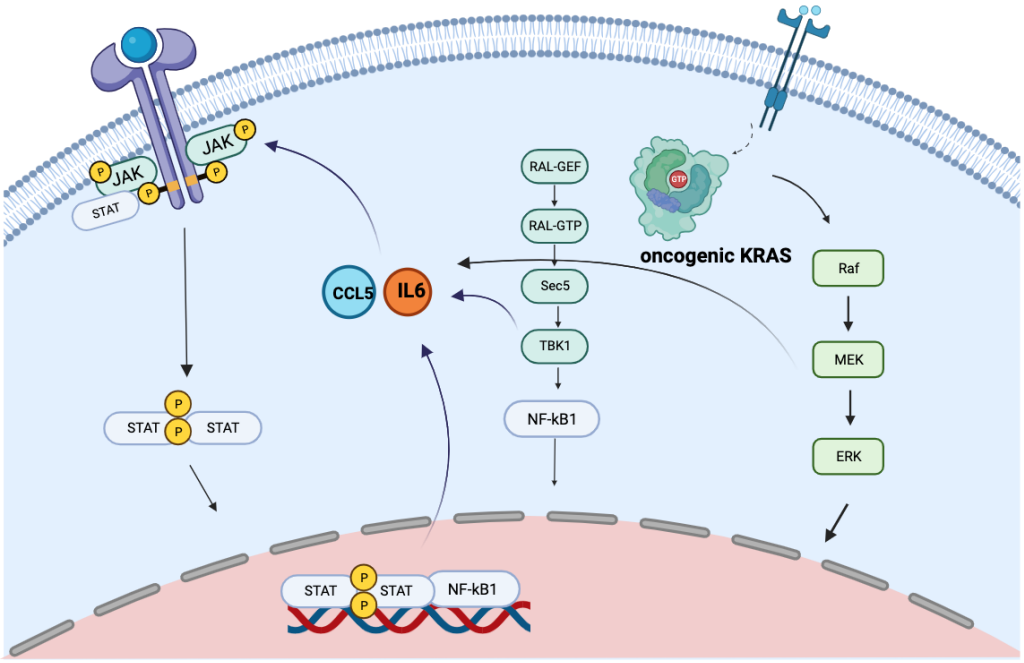

Figure 3: **Oncogenic KRAS-driven inflammation**. Oncogenic KRAS secretes several inflammatory cytokines, such as IL6 and CCL5, which in turn lead to activation of JAK/STAT signaling pathway known to play important role in inflammation and tumorigenesis. Subsequently, activated STATs enhance NF-kB signaling also involved in tumor progression. Created with BioRender.com (www.biorender.com). Adapted from Kitajima, Thummalapalli and Barbie, 2016.

1.9. JAK/STAT signaling pathway

JAK/STAT signaling pathway is evolutionary conserved and it consists of three essential components: a cellular receptor, Janus kinase (JAK) protein and a signal transducer and activator of transcription (STAT) protein. It is involved in many physiological processes including cell survival, proliferation, differentiation, development and inflammation (Nicolas et al., 2012).

JAK represents a family of non-membrane tyrosine kinases composed of 4 main members- JAK1, JAK2, JAK3 and TYK2. While JAK3 is mainly expressed in hematopoietic cells, other three kinases are expressed in almost all tissues. On the other hand, 7 STAT family members have been identified: STAT1, STAT2, STAT3, STAT4, STAT5a, STAT5b and STAT6.

JAK/STAT signaling starts with a ligand binding to the corresponding transmembrane receptor, mostly cytokine and growth factor receptors, causing receptor dimerization and subsequent JAK phosphorylation. Activated JAKs lead to the phosphorylation of tyrosine residues on the catalytic domain of the receptor, which serve as a docking site for STATs. Following JAK-mediated STATs phosphorylation, STATs dissociate from the receptor and form homo- or hetero-dimers. In such form, they translocate to the nucleus, where they can directly bind DNA and regulate gene expression (O'Shea et al., 2015; Hu et al., 2021; Hu et

al., 2023). However, STATs can also form a transcription complex with a non-STAT transcription factor and trigger transcription mediated by STAT as well as synergistically activate transcription by binding to clusters of independent DNA-binding sites (Hu et al., 2021). JAK/STAT is also involved in non-classical signal transduction. Unphosphorylated STATs can induce multiple STAT target gene expression and its activation is not necessarily linked to cytoplasm. Moreover, STATs can localize to mitochondria and protect from apoptosis by inhibiting mitochondrial permeability transition pore opening (Bharadwaj et al., 2020). JAKs, on the other side, can carry out functions in the nucleus independently of STATs involving phosphorylation of histone proteins (O'Shea et al., 2015). This further highlights the complexity of JAK/STAT signaling.

1.9.1. JAK/STAT pathway in diseases

Since JAK/STAT pathway is involved in many physiological processes, its dysregulation is associated with development of variety of diseases. Aberrant JAK/STAT signaling, activating proinflammatory cytokine signaling, disrupts immune balance and contributes to the development of inflammatory and autoimmune diseases, including rheumatoid arthritis, systemic lupus erythematosus and psoriasis as well as cancer progression (Banerjee et al., 2017; Tzeng, I-Tsu Chyuan and Lai, 2021). Efficient treatment of rheumatoid diseases with JAK inhibitors highlights the importance of targeting JAKs to suppress inflammation and opens new possibilities for their therapeutic application in many diseases (Taylor et al., 2023).

1.9.2. JAKs and cancer

Use of JAK inhibitors for hematological disorders, particularly myeloproliferative neoplasms (MPN), caused by activating mutations in JAK2, presents an important therapeutic approach (Kirito, 2022). The identification of JAK2 V617F mutation, which contributes to constitutive activation of JAK/STAT signals and downstream pathways leading to modification of hematopoietic stem cells proliferation rate, is recognized as a critical diagnostic criterion in neoplasms (de Freitas and da Costa Maranduba, 2015). JAK1 somatic mutations have also been observed in myeloproliferative neoplasms (Arulogun et al., 2017). Thus, development of JAK inhibitors followed the discovery of these activating mutations, with ruxolitinib being one of the first clinically approved JAK1/2 inhibitors. Yet, no similar activating mutations have been found in solid cancers (Campbell et al., 2016). Ruxolitinib, however, exhibits immunosuppressive effects, which makes it appealing for autoimmune diseases, but questions its efficacy in cancer treatment (Klein et al., 2021). JAK inhibitors (JAKi) affect different parts of body´s natural defenses including natural killer cells, dendritic cell as well as T helper and regulatory T cells (Elli et al., 2019). Indeed, patients treated with JAKi had

reduced natural killer (NK) cell numbers, which act as a first line of defense against transformed cells, leading to impaired cytokine-mediated NK cells activation and functions (Schönberg et al., 2015). Similarly, blocking JAK/STAT pathway with JAKi, active in metastatic breast cancer, enhanced metastatic burden due to impairment of NK-cell mediated anti-tumor immunity (Bottos et al., 2016).

On the other hand, in the case of myeloid-derived suppressor cells (MDSCs), able to efficiently inhibit T cell function and thus facilitate tumor escape, inhibition of JAK/STAT signaling pathway was proposed as a possible therapeutic option (de Haas et al., 2016). In fact, JAK/STAT3 inhibitors blocked angiogenesis and reduced MDCs in the TME in the head and neck cancer as well as resulted in the loss of cancer stem-like characteristics and reduced tumor burden in ovarian cancer (Liu et al., 2018; Abubaker et al., 2014). This further highlights the importance of IL6/JAK/STAT3 signaling pathway in cancer progression. Additionally, activation of JAK2/STAT5 pathway in prostate cancer is linked to the high-grade prostate cancer, and this connection offers a potential approach for pharmacological intervention in the clinical progression of prostate cancer (Tan and Nevalainen, 2008). Preclinical studies also indicate that inhibiting this pathway results in extensive cell apoptosis and reduced tumor burden (Beinhoff et al., 2021).

In the case of lung cancer, JAK inhibition has been shown to block IFNγ induced immune escape from NK cells in NSCLC cells (Okita et al., 2019). Moreover, targeting JAKs sensitized human EGFR-mutated NSCLCs by overcoming resistance to TKIs (Kim et al., 2020). Even though IL6/JAK/STAT3 pathway has been associated with KRAS-mutated LUAD, the role of JAK/STAT in this type of cancer has not been extensively researched.

1.10. Rationale of the thesis

Lung cancer continues to be the leading cause of cancer-related mortality globally. Among the most common type of lung cancer, NSCLC, adenocarcinomas are the predominant subtype. While EGFR tyrosine kinase inhibitors are established as the standard treatment for EGFR-mutated lung adenocarcinoma, development of KRAS inhibitors has been less successful. Treatment strategy for this type of cancer follows the one of non-oncogene driven NSCLC, including chemotherapy, radiation and immunotherapy. Currently, there are two clinically approved KRAS inhibitors targeting G12C mutation. However, current treatments have failed to benefit KRAS mutant patients, suggesting there is an urgent need for novel treatment strategies. Since the tumorigenesis of KRAS is closely associated with inflammatory process and JAKs act as a core molecules in inflammatory events, JAK/STAT pathway presents an attractive therapeutic target for KRAS-mutated LUAD.

1.11. Preliminary data

The connection between KRAS-mutated LUAD and JAK/STAT signaling pathway has previously been established in our lab and published by Mohrherr et al.

Namely, to investigate influence of JAK1 and JAK2 on KRAS-mutated LUAD progression, publicly available mRNA expression data set GSE75037 revealed increased JAK1/2 expression levels in patients with more advanced disease compared to stage I classified KRAS-mutated LUAD, which reached significance for JAK1 (Figure 3a). Additionally, activation of JAK/STAT pathway has been found in patients with more advanced LUAD as determined by GSEA (Figure 3b).

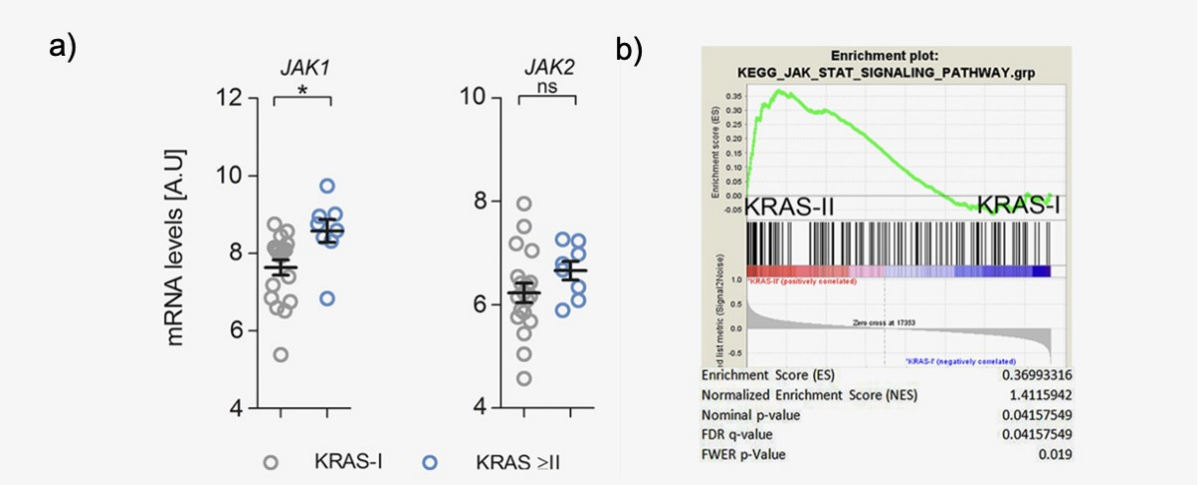

Figure 4: **JAK mediated signaling in KRAS-mutated LUAD**. a) Relative JAK1 and JAK2 mRNA expression levels in human KRAS-mutated LUAD comparing stage I patients versus stage II or higher. b) JAK/STAT pathway signature gene set comparing human KRAS-mutated tumors of stage I versus stage II using tumors versus healthy parenchyma mRNA expression ratios. Data in A) and B) extracted from the Gene Expression Omnibus (GSE75037). *p<0.05 (Mohrherr et al., 2019).

Next, to assess effect of pharmacological JAK inhibition on KRAS-driven tumor progression, immunodeficient NOD scid gamma mice were subcutaneously transplanted with human LUAD cell line, A549 ($KRAS^{G12S}$) and treated with selective JAK1/2 inhibitor ruxolitinib. The treatment resulted in significant reduction of tumor growth (Figure 5a-c). To verify inhibition of JAK1/2, activation of its downstream effector, activated STAT3, was evaluated which showed significant reduction upon treatment as confirmed by immunohistochemistry (Figure 5d).

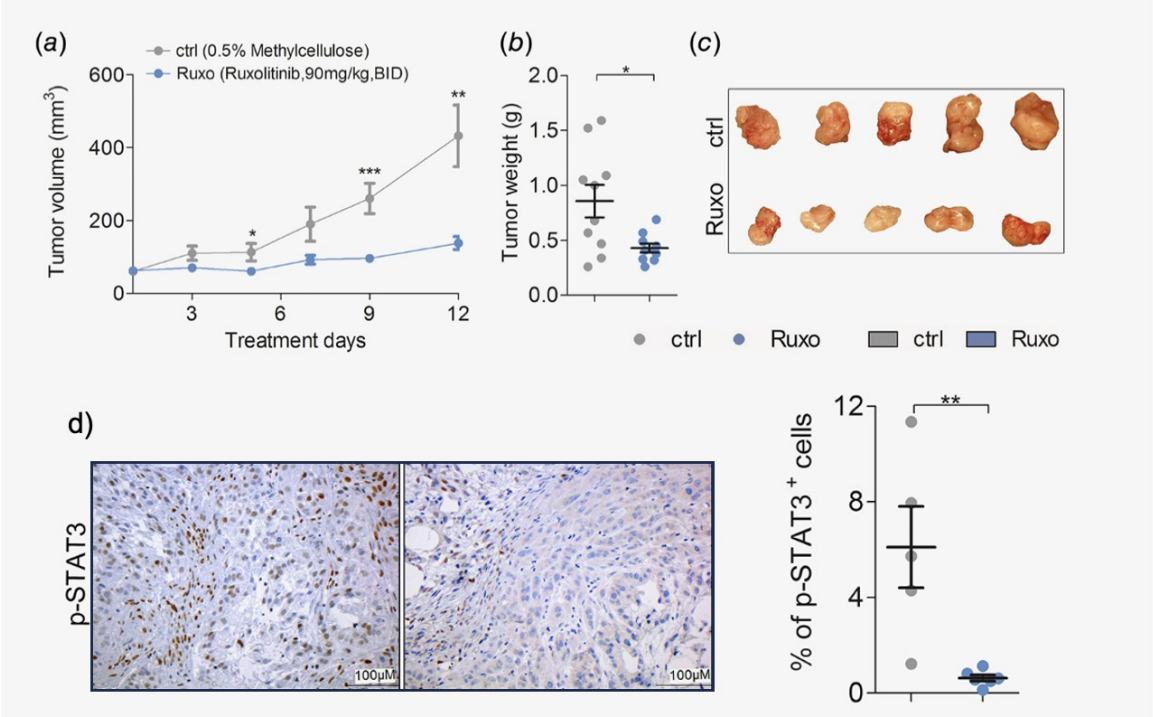

Figure 5: **Inhibiting JAKs hinders the growth of human KRAS-mutated LUAD cells in vivo.** a) Mean tumor volume of NOD scid gamma mice transplanted with A549 human KRAS LUAD cells and treated twice daily with 90mg/kg ruxolitinib or vehicle control. b) Weight of tumors at the conclusion of the study. c) Representative pictures of subcutaneous tumors d) Immunohistochemical staining and quantification for pSTAT3 of A549 derived xenograft tumors treated with ruxolitinib or control. *p<0.05, ***p<0.01 (Mohrherr et al., 2019).

Moreover, considering ruxolitinib immunosuppressive effects and its controversial role in solid tumors, effect of JAK inhibition on KRAS-driven LUAD was further assessed in immunocompetent mouse model of autochthonous KRAS-driven LUAD, KRAS $^{LSL\text{-}G12D}$:p53 $^{fl/fl}$ (KP). These mice were inhaled with Cre-recombinase expressing adenovirus (Ad. Cre) which led to KRAS^{G12D} activation in lung epithelial cells as well as p53 deficient LUADs. KP mice were treated 1 week post tumor induction with JAK1/2 inhibitor ruxolitinib or vehicle control for 10 weeks after which their lungs were analyzed. A significant decrease in tumor burden was observed in ruxolitinib treated mice compared to control mice as shown by reduced lung to body weight ratio as well tumor to lung area ratio (Figure 6a-b). Additionally, RNA-seq revealed that JAK inhibition abrogated expression of key proinflammatory and pro-tumorigenic factors including IL6, TNF*α* and CXCL1 (Figure 6c). On the other hand, flow-cytometric analysis of lung tumors revealed significant reduction of tumor promoting granulocytic CD45$^+$CD11b$^+$LY6G$^+$ and monocytic CD45$^+$CD11b$^+$LY6C$^+$ MDSCs. Moreover, the number of tumor promoting CD45$^+$CD11b$^+$CD206$^+$ M2 macrophages was lowered upon JAK1/2 inhibition as well as number of NK and infiltrating CD8$^+$ and CD4$^+$ T cells (Figure 6d).

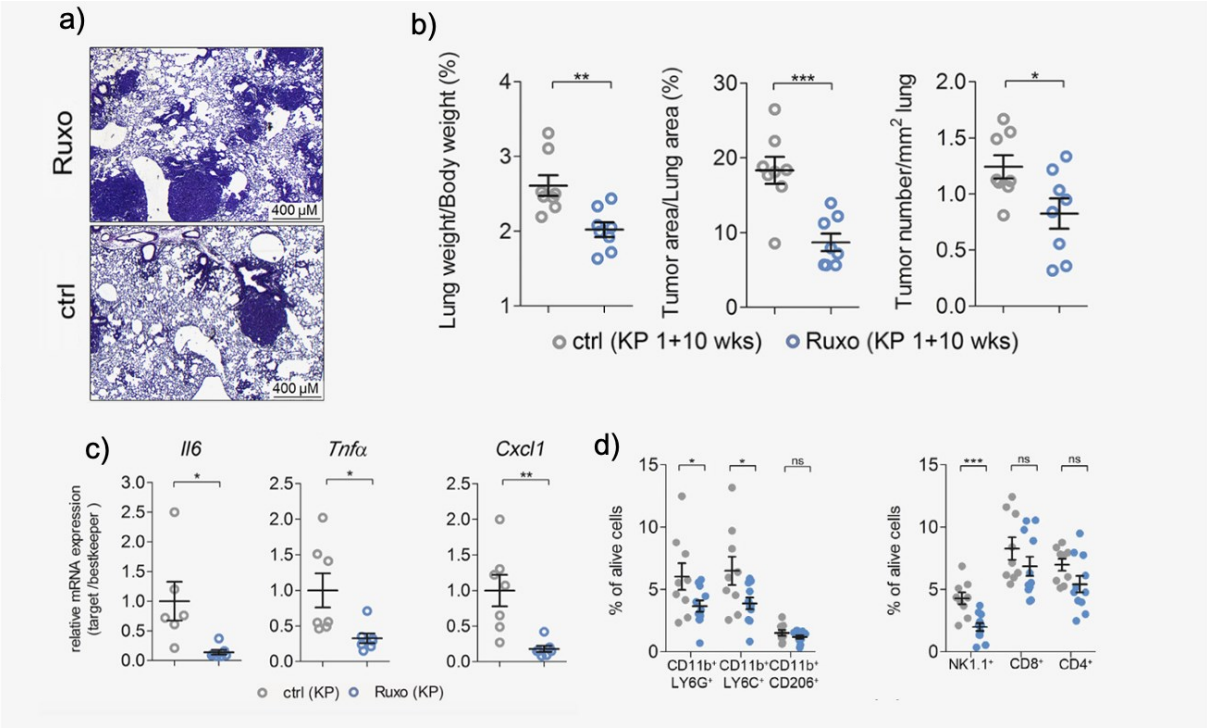

Figure 6**: Ruxolitinib reduces tumor progression of KRAS autochthonous mouse model.** a) Hematoxylin and eosin staining of lung sections of KRAS $^{LSL\text{-}G12D}$:p53$^{fl/fl}$ (KP) mice treated with 90mg/kg ruxolitinib or vehicle control twice daily for 10 weeks. b) Quantification of H&E staining of lung sections of KRAS $^{LSL\text{-}G12D}$:p53 $^{fl/fl}$ treated with ruxolitinib or vehicle control. c) IL6, TNF*α* and CXCL1 relative mRNA expression levels in KP tumors upon treatment with ruxolitinib or vehicle control. d) Flow cytometric analysis depicting percentages of myeloid (left) and lymphoid (right) cells upon ruxolitinib or vehicle control treatment. *p<0.05, **p<0.01, ***p<0.001 (Mohrherr et al., 2019).

1.12. Aim of the thesis

Previously published data demonstrated that KRAS-mutated LUAD responded to JAK1/2 inhibitor ruxolitinib. However, inhibition was assessed in T-cell independent mouse model where infiltrating CD8$^+$ T cells play a minor role. Considering immunosuppressive role of ruxolitinib, which was also shown by reduced T cell infiltration in tumors, it is difficult to assess potential antitumoral effects and its influence on immune surveillance. Thus, the aim of this thesis is to elucidate the role of JAK1 and JAK2 in T-cell dependent experimental models of KRAS-driven LUAD, which more closely resemble human tumors.

2. MATERIALS AND METHODS

2.1. Cell culture

2.1.1. Cell line

KPO cells were previously derived from tumor bearing KPO mouse model 10 weeks post tumor initiation, which was generated by breeding $KRAS^{LSLG12D}$:$p53^{fl/fl}$ mice with mice harboring reversely oriented GFP-ovalbumin (GFP-OVA) construct. Inhalation with Cre-recombinase expressing adenovirus (Ad. Cre) activated $KRAS^{G12D}$ mutation in lung epithelial cells, p53 deletion as well as expression of GFP-OVA fusion protein facilitating antigen presentation to T cells.

2.1.2. Culturing cells

Isolated cells were cultured in RPMI-1640 (Sigma-Aldrich) containing L-glutamine and sodium bicarbonate, supplemented with 10% FBS (Capricorn Scientific) and 1% Penicillin-Streptomycin (Sigma-Aldrich), referred as complete growth medium. They were incubated in humidified incubator containing 5% CO_2 at 37°C. For cell detachment, trypsin-EDTA solution (Sigma-Aldrich) was used. Cells, cultured in 10 cm dishes, were washed with 1xPBS (Gibco) after which 2 ml of trypsin was added and cells incubated in 5% CO_2 incubator at 37°C for approximately 10 minutes. Trypsinization was stopped by adding fresh growth medium and predetermined cell count was carefully transferred to a new dish containing complete growth medium. All cells were used within 15 passages for experiments.

2.1.3. Counting cells

Cells were counted using DeNovix cell counter by diluting cells with Trypan Blue (Gibco) at 1:1 ratio using appropriate counting protocol.

2.1.4. Freezing cells

Cells were trypsinized and centrifuged at 300 x g for 5 min. Following cell counting, corresponding cell numbers were collected by centrifugation, and cell pellet was resuspended in RPMI-1640 containing L-glutamine and sodium bicarbonate, supplemented with 20% FBS, 10% DMSO (Sigma-Aldrich) and 1% Penicillin-Streptomycin. Cells were stored in cryovials at -80°C or in liquid nitrogen for a long term storage.

2.1.5. Thawing cells

Cells, previously stored in liquid nitrogen and kept in 2 ml cryovials, were left to thaw on room temperature. Following transfer to a 15 ml tube, 10 ml complete growth medium was added dropwise to the cells. Cells were then centrifuged at 300 x g for 5 min. Obtained cell pellet was resuspended in complete medium and cells were seeded to appropriate culture dish.

2.2. Crispr/Cas9

2.2.1. Transfection and Puromycin Selection

To perform CRISPR/Cas9 knockout of JAK1, JAK2 and JAK1/2 in KPO cells, gRNAs (Table 1) targeting these genes were coupled to a Cas9 expression plasmid conveying puromycin resistance pSpCas9(BB)-2A-Puro V2.0 (Addgene). As a positive control, pSpCas9(BB)-2A-GFP (Addgene) plasmid was used and an empty vector as a negative control.

Gene	Sequence (5´-3´)	Exon
mJak1	TCTCATCGTACAGGGCGAAG	4
mJak2	CAGATACGGAGTGTCCCGTG	5

Table 1: gRNAs targeting JAK1 and JAK2

Prior to transfections, KPO cells were seeded in 24-well plate in triplicates ($5x10^5$ cells/well), to achieve approximately 80% confluency by the next day. Cells were transfected with plasmids using Lipofectamine LTX (Invitrogen). Per well, 500 ng of each plasmid was mixed with 100 µL Opti-MEM (Invitrogen). Next, 0.5 µL of Plus Reagent (Invitrogen) was added and mixture was flipped and spined down to ensure retrieval of any remaining fluid. This was followed by 5 min incubation at room temperature. After addition of 2 µL of Lipofectamine LTX, mixture was spined down again and incubated for 25 min at room temperature. Complete growth medium in 24-well plates was changed to 1 mL DMEM (Gibco) supplemented with 10% FBS. Following incubation, 105 µL of transfection mix was added dropwise to each well ensuring mixture was distributed equally. When two plasmids were co-transfected for double knockout, each plasmid was mixed with 50 µL Opti-MEM and Plus Reagent was added to both. Afterwards, two solutions were combined, and it was continued as described previously. After 24 hours, transfection efficiency was estimated by checking GFP-positive cells in control wells. Cells were washed with 1xPBS and 1 mL of RPMI-1640 medium without antibiotics was added to each well. Next, increasing concentrations of puromycin (5-20 µg/ml) (InvivoGen) were pipetted in the wells. After 2 days of selection, puromycin was removed and cells were

washed with 1xPBS. Finally, complete growth medium was added to each well. Once the cells were confluent, they were expanded to 6-well plate and later to 10cm plate.

2.2.2. Single clone generation

To obtain single clones from pool of $KPO^{\Delta JJAK1/2}$ cells, 50 cells were seeded from 10 cm plate to 96-well plate and incubated at 37°C and 5% CO_2 until first single clones appeared. Wells containing single clones were washed with 1xPBS, trypsinized and expanded to 24-well plate followed by expansion to a 6-well plate once confluent.

2.2.3. DNA Isolation

Cells were harvested from 6-well plates and centrifuged at 300 x g for 5 minutes. Obtained cell pellets were washed with 1xPBS. After supernatant was removed, pellet was dissolved in 200 µL lysis buffer (Table 2) and incubated overnight shaking at 55°C /800 rpm.

Reagent	Concentration (mM)
Tris-HCl pH 8	50
EDTA	100
NaCl	100
SDS	1%

Table 2: DNA lysis buffer for DNA isolation

Next, 85 µL NaCl was added to the cells followed by tube inversion and centrifugation at 16000 x g for 10 mins. Supernatant was then transferred into a new tube and 250 µL isopropanol (Roth) was added and mixed by inversion. After 5 min centrifugation at 16000 x g, pellet was washed with 1 mL 70% EtOH. Following final centrifugation for 5 min at 16000 x g, supernatant was removed, and dry pellet was resuspended in 50 µL nuclease-free water (Promega). DNA concentration was measured using Tecan Infinite^{R} 200 Pro plate reader.

2.2.4. Polymerase Chain Reaction Analysis

Amplification of the genomic region encompassing the break site was performed to assess genome editing using primers listed in Table 3. To achieve this, 100 ng genomic DNA was diluted in ddH_2O to a final volume of 17.9 µL. Next, 7.1 µL master mix (Table 4) was added in each well. Reaction mixture was prepared on ice and run on PCR cycler using program listed in Table 5.

Gene		Sequence (5´-3´)
mJak1	Forward	TCTGTTCCCTTGCTGTGATTTA
	Reverse	GGAGGGCTGAGCACTTATTT
mJak2	Forward	CAAACTAAAGAAGGCGGGTA
	Reverse	TGACATTTTCTCGCTCAACA

Table 3: Primers targeting JAK1 and JAK2

Reagents	Volume (µL)
Primer mix (fw+rev, 10uM)	1
5x GoTaq buffer	5
dNTPs (5mM)	1
GoTaq G2 DNA Polymerase	0.1

Table 4: Master mix for polymerase chain reaction

Temperature (°C)	Time (s)	
95	120	
95	30	X38
58	30	
72	45	
72	120	
4	hold	

Table 5: Thermocycler program for JAK1/2 amplification

2.2.5. Agarose Gel Electrophoresis

To analyze amplified PCR product, 2% agarose gel was prepared in TAE buffer with an addition of 2 µL per 100 mL gel of SYBR safe (Peqlab). Once the gel solidified, 3 µL of 1kbp Gene Ruler (Thermo Fisher Scientific) and 10 µL of amplified PCR product were loaded onto the gel. Gel was run at 120V for 30 minutes and imaged using ChemiDoc MP Imaging System (Bio-Rad).

2.2.6. Purification of Amplified DNA Fragments

Amplified PCR products were purified using NucleoSpin® Gel and PCR Clean up following manufacturer´s instructions. One volume of sample was mixed with 2 volumes of NTI buffer. Sample was then loaded into provided column placed into a collection tube followed by

centrifugation for 30 s at 110000 x g. After discarding flow-through, column was washed with 700 µL NT3 buffer and centrifuged for 30 s at 11000 x g. Final centrifugation step for 1 min at 11000 x g ensured that NT3 buffer was removed completely. Column was then placed in a new microcentrifuge tube and DNA elution with 15 µL buffer NE was accomplished by centrifugation at 11000 x g for 1 minute.

2.2.7. Sanger Sequencing Sample Preparation

To assess knockout efficiency, 100 ng of purified PCR product was diluted to a final volume of 10 µL. Prior to sending samples for Sanger sequencing, 4 µL of either forward or reverse primer (Table 3) was added to each sample. Analysis of indels and edits for pools as well as single clones was performed using online TIDE software (https://tide.nki.nl/).

2.3. Western Blot Analysis

Cells were seeded in 6-well plate ($4.5x10^5$ cells/well) and incubated at 37°C in 5% CO_2 incubator for 24 hours. Following 24-hour cell starvation with 0.2% RPMI-1640, cells were treated with 5 ng/mL IFNγ diluted in RPMI-1640 growth medium for 15 minutes. Next, they were washed with ice-cold PBS. To detach cells, 150 µL lysis buffer (Table 6) containing 1% PMSF (Fluka) was added to each well, followed by cell detachment using cell scraper.

Reagent	Volume (mL)	Concentration (mM)
Tris pH 7.5	1	20
NaCl (5M)	1	100
Na_3VO_4 (0.2M)	0.25	1
NaF (0.5M)	10	100
Glycerol-2-phosphate (0.2M)	5	20
EDTA (0.25M)	0.5	2.5
EGTA (0.25M)	0.2	1
NP-40	0.5	1%

Protease inhibitor	5 tabs	
ddH_2O	31.55	

Table 6: Protein lysis buffer

Lysates were then transferred to a new pre-cooled centrifuge tube and centrifuged at maximum speed for 10 minutes at 4°C. The resulting supernatant was transferred to a new tube. Protein concentration was determined by BCA (Biovision) in 96-well plate. Samples were diluted with lysis buffer at 1:5 ratio to a final volume of 25 µL and 25 µL of BSA standard solutions ranging from 0 to 2 mg/mL were pipetted into separate wells of a 96-well plate. Next, 200 µL of BCA working reagent was added to each well. Following 30 min incubation at 37 °C, absorbance was measure using Tecan Infinite^R 200 Pro plate reader. The standard curve was generated by plotting the absorbance values of BSA standards measured at 562nm.
Samples were then diluted to 20 µg with lysis buffer with an addition of 5x Laemmli buffer (Bio-Rad). Stacking and separating gel (10%) were prepared as indicated in Table 7. Electrophoresis chamber (Bio-Rad) was assembled and filled with running buffer (Table 8). Following 95°C incubation for 5 minutes, 10 µL of each sample was loaded onto SDS-page including 3 µL protein ladder (Invitrogen). Gels were run at 90V to let samples stack before increasing voltage to 120V.

	Volume (mL)	
Reagent	Separating gel (20mL)	Stacking gel (6mL)
H2O	10.6	4.1
30% Bis-Acrylamide	4	1
1.5M Tris (pH 8.8/pH 6.8)	5	0.75
10% SDS	0.2	0.06
10% APS	0.2	0.06
TEMED	0.016	0.005

Table 7: 10% separating and 6% stacking gel

Reagent	Volume (mL)
10xTGS	100
ddH2O	900

Table 8: Western Blot running buffer

After successful electrophoresis, transfer was performed. Proteins were moved from the gel to a PVDF transfer membrane (Amersham™Hybond™) by assembling western blot sandwich in the following way: blotting paper, PVDF membrane, gel and a blotting paper in a container filled with the provided transfer buffer (Bio-Rad). Trans-Blot® SD Semi-Dry Cell (Bio-Rad) was used for transfer for 10 minutes at 15V. Next, membrane was stained with Ponceau solution (Table 9) until bands became visible and de-stained by washing with TBST buffer (Table 10). Starting from this step, membrane was moved to a 50 mL falcon tube and all further steps were performed within it.

Reagent	Mass (g)/ Volume (mL)	Concentration
Ponceau S (760.57 g/mol)	5	1.3 mM
Acetic acid (glacial)	25	5%
ddH2O	475	

Table 9: Ponceau S staining solution

Reagent	Volume (mL)
10x TBS	100
ddH2O	899
Tween 20	1

Table 10: TBST Buffer

Prior to primary antibody incubation, to prevent any unspecific antibody binding, membrane was incubated with blocking solution (Table 11) for 1 hour at room temperature. Primary antibodies, as listed in Table 12, were diluted in 2.5% B-TBST and incubated overnight at 4°C.

Reagent	Amount
Bovine serum albumin (BSA)	5g
TBST	100ml

Table 11: 5% B-TBSTS blocking solution

Antibody	Dilution	Company
Jak1 (6G4) Rabbit mAb	1:1000	Cell Signaling Technology
Jak2 (D2E12) Rabbit mAb	1:1000	Cell Signaling Technology
Stat1(D1K9Y) Rabbit mAb	1:1000	Cell Signaling Technology
Stat3 (124H6) Mouse mAb	1:1000	Cell Signaling Technology
Phospho-Stat1(Ser727) (D3B7) Rabbit mAb	1:1000	Cell Signaling Technology
Phospho-Stat3(Tyr705) (M9C6) Mouse mAb	1:1000	Cell Signaling Technology
GFP (D5.1) Rabbit mAb	1:1000	Cell Signaling Technology
HSC 70 Antibody (B-6)	1:1000	Santa Cruz
Anti-rabbit/Anti-mouse HRP Secondary AB	1:3000	Cell Signaling Technology

Table 12: Primary and secondary antibodies used for western blot analysis

After incubation, membrane was washed three times with TBST for 5-15 minutes. Secondary antibody, compatible with the primary, was diluted in 2.5% B-TBST and added to the membrane. Following 1 hour incubation at room temperature, membrane was washed three times with TBST for 5-15 minutes. Pierce™ ECL Plus substrate (Thermo Fisher Scientific) was used for protein detection and membrane was visualized using ChemiDoc MP Imaging System (Bio-Rad). To incubate membrane with another primary antibody, membrane was washed three times with TBST, stripped with stripping buffer (Table 13) two times for 10 minutes and finally washed with TBST. Prior to antibody addition, membrane was incubated with blocking solution for 1 hour at room temperature.

Reagent	Amount
Glycine	15g
SDS	1g
Tween 20	10ml
ddH2O	980ml

Table 13: Western Blot stripping buffer

2.4. Real Time Quantitative Polymerase Chain Reaction

2.4.1. RNA isolation

Cells were seeded in 24-well plates ($10x10^4$ cells/well). Following stimulation of the cells with 5 ng/mL IFNγ or increasing concentration of isolated lung fluid (50-200 µg/mL) following day for 4 hours, RNA was isolated using E.Z.N.A.® Total RNA KIT I (Omega) as per manufacturer's instructions. Cells were disrupted and harvested using 350 µL TRK lysis buffer (Omega) per well (20 µL β-mercaptoethanol (Sigma) was added per 1ml TRK lysis buffer). To homogenize the cells, cell lysate was loaded into the provided homogenizer mini column inserted into collection tube and centrifuged at maximum speed for 2 minutes. Next, 1 volume of 70% ethanol was added to the homogenized lysate and samples were vortexed. Mixture was then transferred to the provided HiBind® RNA Mini Column and centrifuged at 10000 x g for 1 minute. Filtrate was discarded and the column was washed with 500 µL RNA Wash Buffer. Following centrifugation at 10000 x g for 30 seconds, filtrate was discarded and 500 µL RNA Wash Buffer II was added to the column. After centrifugation at 10000 x g for 30 seconds, second RNA Wash Buffer II step was repeated. Final centrifugation step at maximum speed for 2 minutes was performed to dry the column. RNA was then eluted with 40 µL nuclease-free water into a clean microcentrifugation tube by centrifugation at maximum speed for 2 minutes. RNA concentration was measured using Tecan Infinite^R 200 Pro plate reader.

2.4.2. Complementary DNA (cDNA) Synthesis

To synthesize DNA from RNA template, Bio-Rad iScript cDNA kit was used. For the reaction, 1000 ng RNA was diluted in nuclease-free water and added to the mixture consisting of 4 µL 5x buffer (Bio-Rad) and 1 µL reverse transcriptase (Bio-Rad). Reaction was then run on Eppendorf thermocycler using program depicted in Table 14. Synthesized cDNA was diluted in nuclease-free water at 1:20 ratio.

Temperature (°C)	Time (min)
25	5
46	20
95	1
4	hold

Table 14: Thermocycler program for cDNA synthesis

2.4.3. Real-time quantitative PCR Analysis

Using white qPCR 96-well plate (Thermo Scientific), 5 µL cDNA of each sample was pipetted in triplicates together with 10 µL Bio-Rad qPCR reaction mix (Table 15) using primers listed in Table 16. Reaction was run on Bio-Rad CFX Connect™ Thermocycler using program as shown in Table 17. Obtained qPCR results were normalized to m28S housekeeping gene and analyzed using Pfaffl method (Pfaffl, 2001).

Reagent	Volume (µL)
iTaq Universal SYBR Green Supermix (2x)	7.5
Primer mix	0.75
ddH2O	1.75

Table 15: GoTaq qPCR Master mix

Gene	Sequence (5´-3´)
mJak1	Forward CTTTCGGTGCCTCTCCTTAG
	Reverse AGAGCTGATCACTTCCGTGT
mJak2	Forward CAAACTAAAGAAGGCGGGTA
	Reverse TGACATTTTCTCGCTCAACA
mH2-kb (MHC-I)	ForwardGCTGGTGAAGCAGAGAGACTCAG
	Reverse GGTGACTTTATCTTCAGGTCTGCT
hCD274 (PD-L1)	Forward CTGAATTGGTCATCCCAGAACTAC
	Reverse TGGCTCCCAGAATTACCAAGTG
mCXCL10	Forward ATCATCCCTGCGAGCCTATCCT
	Reverse GACCTTTTTTGGCTAAACGCTTTC
m28S	Forward ATACCGGCACGAGACCGATAGTCA
	Reverse GCGGACCCCACCCGTTTACCTC

Table 16: Primers used for RTqPCR

Temperature (°C)	Time (s)	
95	30	
95	5	39x
60	30	
65	5	
65-95 in 0.5	5	

Table 17: Bio-Rad CFX Connect™ Thermocycler program

2.5. Cell-based assays

2.5.1. Cell proliferation assay

For cell proliferation assay, knockout cell lines were seeded in 6-well plate in quadruplicates ($2.5x10^4$ cells/well) and incubated for 72 and 96 hours in humidified incubator containing 5% CO_2 at 37°C. Following two incubation periods, cells were trypsinized and counted by mixing 1 part of trypan blue (Gibco) with 1 part of cell suspension using DeNovix cell counter.

2.5.2. AlamarBlue assay

KPO cells were seeded in 96-well plate ($4x10^3$ cells/well). Following overnight incubation at 37°C and 5% CO_2, cells were treated with increasing concentrations of JAK1/2 inhibitor ruxolitinib (LC Labs) with concentrations ranging from 0 to 400 µM. After 48-hour incubation, AlamarBlue (Invitrogen) was added in an amount equal to 10% of the volume in the well. Plate was incubated for 4 hours at 37°C and 5% CO_2 and cell viability was determined by measuring absorbance at 560 and 600 nm using Tecan Infinite^R 200 Pro plate reader.

2.5.3. In vitro T cell killing assay

2.5.3.1. $CD8^+$ T cell isolation

Using MACS Miltenyi Biotec $CD8^+$ T cell isolation kit, cytotoxic $CD8^+$ T cells were isolated from spleen of OT I mouse with transgenic T cell receptor that recognizes ovalbumin residues 257-264 following manufacturer´s instructions. Previously isolated splenocytes (see 2.7.2.1. Splenocyte isolation) were counted using DeNovix cell counter and cell pellet was resuspended in 40 µL/10^7 cells MACS buffer (Table 18).

Reagent	Concentration
Bovine serum albumin (BSA)	0.5%
EDTA	2mM
PBS	

Table 18: MACS buffer for CD8+ T cell isolation

Next, 10 µL/10^7 cells Biotin-AB cocktail (Miltenyi Biotec) were added to the cells, mixed well and incubated 5 min on ice. Additional 30 µL MACS buffer were added together with 20 µL Anti-Biotin Microbeads (Miltenyi Biotec) followed by 10 min incubation on ice. Cell suspension was then applied onto LS column in the magnetic field of MidiMACS separator previously primed with 3 mL of MACS buffer. Following additional washing step with 3 mL of MACS buffer, flow-through was collected in a new tube resulting in enriched $CD8^+$ T cells. Cells were then centrifuged at 300 x g for 5 minutes and the resulting pellet was resuspended in RPMI-1640 medium containing L-glutamine and sodium bicarbonate, supplemented with 10% FBS, 1% P/S, 1% MEAA (Corning), 0.1% β-mercaptoethanol and 1% sodium pyruvate (culture medium for T cells). To increase viability and cytotoxicity, isolated $CD8^+$ T cells were cultured in culture medium for T cells supplemented with 1 ng/mL IL7 and IL15 for 4 days. Next, $CD8^+$ T cells were counted and cocultured with cancer cells seeded in 12-well plate in triplicates ($1.5x10^4$/well) at 1:10 ratio for 5 days. In vitro cell killing was assessed based on colony formation assay.

2.5.4. Colony formation assay

Previously seeded KPO/KP cells in 12-well plate cocultured with T-cells were washed 2 times with 1xPBS followed by cell fixation with 2-3 mL of 4% ROTI®Histofix (Roth) for 15 minutes at room temperature. After carefully removing histofix, cells were then stained with 0.01% crystal violet for 2 hours at room temperature. Next, crystal violet was removed, and plates were washed with water and left to air-dry at room temperature. Colonies were counted using ImageJ.

2.6. Animal husbandry and experiments

2.6.1. Mouse strains

C57BL6/N mice

C57BL6/N is an inbred mouse strain characterized by responsive immune system. Within the scope of this thesis, it is used for subcutaneous and intratracheal transplantation experiments. Mice were obtained from Jackson Laboratory.

2.6.2. Subcutaneous transplantation

For subcutaneous injections using previously isolated KPO cell line, $1x10^6$ cells resuspended in 50 µL aliquots of RPMI-1640 medium without supplements were mixed 1:1 with Matrigel (Corning) on ice. Cells were then injected in the right flank of C57BL6/N mice older than 6 weeks. Tumor volume measurement was performed using a caliper and calculated using [(length × width^2) × 0.52] formula. At the experimental endpoint, subcutaneous tumors were excised and used for histological and flow cytometric analysis.

2.6.3. Oral gavage

C57BL6/N mice received 90 mg/kg JAK1/2 inhibitor ruxolitinib (LC Labs) resuspended in 0.5% methylcellulose (prepared with the addition of 0.9% NaCl and 0.05% Tween 80) or control (0.5% methylcellulose) twice a day 7 days per week via oral gavage.

2.6.4. Intratracheal transplantation

For intratracheal transplantations, C57BL6/N mice older than 6 weeks of age were transplanted with $1x10^6$ knockout cell lines resuspended in 50 µL aliquots of RPMI-1640 medium without supplements together with 2 µL 250mM EDTA per mouse. Prior to this, mice were injected with ketamine/xylazine solution (Livisto) subcutaneously into the flank for anesthetization (1/10 of the weight of the mouse was used for anesthetization). Transplantation was performed by fixing mouse using a string over upper incisors and light source near the lungs to identify the opening of the trachea. End of the catheter needle was removed, and it was smoothly inserted in the trachea checking the placement by attaching 1 mL syringe with a drop of water to the catheter. Once cell suspension was delivered, an empty 1 mL syringe was attached and 300 µL of air was dispensed into the catheter to ensure equal distribution of tumor cells in the lung. Mice were kept on the heating table until waking up. Upon completion of the experiment, lungs were perfused, harvested and sent for histological analysis.

2.7. Flow Cytometric Analysis

2.7.1. Cultured cells

Cells were seeded in 6-well plate ($4x10^5$ cells/well) and incubated for 24 hours at 37 °C and 5% CO_2. Following 24-hour starvation with 0.2% RPMI-1640, cells were treated with 5 ng/mL IFNγ for 24 hours and harvested in 1 mL ice-cold PBS using cell scraper. After transfer to the FACS tubes, cells were centrifuged at 300 x g for 5 minutes and supernatant was removed.

For each sample, 1 mL of fixable viability dye (Invitrogen) diluted in 1xPBS at 1:2000 ratio was added to the cells followed by 30 min incubation at 4°C. Cells were then washed with 2 mL of FACS buffer (Table 19), centrifuged at 300 x g for 5 minutes and supernatant was removed.

Reagent	Volume (mL)
FBS	10
1xPBS	500
EDTA (250mM)	2

Table 19: 2% FACS Wash Buffer

Next, 200 µL of Fc block (anti-mouse CD16/32, BioLegend) diluted in FACS buffer at 1:200 ratio was added to the cells, samples were vortexed and incubated for the next 30 minutes at 4°C. Following washing step with 2 mL FACS buffer and centrifugation, cells were incubated with 100 µL of antibody mix (Table 20) for 30 minutes at 4°C.

Antibody	Fluorophore	Dilution	Company
MHC Class I (H-2Kb) Monoclonal Antibody	APC	1:400	Invitrogen
D274 (PD-L1, B7-H1) Monoclonal Antibody	PE-Cyanine	1:400	Invitrogen

Table 20: Antibodies used for FACS analysis of cultured cells

After incubation, cells were washed with 2 mL FACS buffer. Resulting cell pellets were resuspended in 200 µL FACS buffer and filtered through a 70 µm cell strainer before pipetting the samples in a 96-well plate together with the controls (unstained, full stain, single stains as well as fluorescence minus one (FMOs)). Samples were measured using Cytoflex Flow Cytometer (Beckman Coulter).

2.7.2. Spleen and subcutaneous tumors

2.7.2.1. Splenocyte isolation

Spleens, harvested from C57BL6/N mice treated with ruxolitinib, were smashed through a 70 µm cell strainer in a dish containing 10 mL RPMI-1640 growth medium using the flat part of 2 mL syringe. Cell suspension was then transferred through the same cell strainer into the falcon tube and cells were collected by centrifugation at 300 x g for 5 minutes. Cell pellet was resuspended in 1 mL ACK Lysing buffer (Lonza) for 5 minutes to lyse red blood cells. Reaction

was stopped by adding 20 mL medium followed by centrifugation. White blood cell pellet was resuspended in RPMI-1640 complete growth medium and cells were moved to FACS tubes. It was then proceeded as described in 2.7.1. by staining cells for flow cytometric analysis using antibodies listed in Table 21.

2.7.2.2. Cells isolation from subcutaneous tumors

KPO subcutaneous tumors, harvested from C57BL6/N mice, were dissected and transferred to a centrifuge tube containing 5 mL complete growth medium supplemented with 50 µL collagenase (Thermo Fisher Scientific) and 0.5 µL DNase (Sigma-Aldrich) per tumor, followed by 1-hour incubation at 37°C. Subsequently, cell suspension was filtered through 70 µm cell strainer further homogenizing the tissue and strainer was rinsed with additional 10 mL complete growth medium. Cells were collected by 5 min centrifugation at 300 x g and cell pellet was washed with complete growth medium followed by transfer to the FACS tubes. Subsequently, cells were stained for flow cytometric analysis as described in 2.7.1. using antibodies listed in Table 21.

Antibody	Fluorophore	Dilution	Company
Viability Dye	eF450	1:2000	Invitrogen
CD45	APC-Cy7	1:400	BD Pharmingen
CD3	FITC	1:400	eBioscience
CD8	AF700	1:400	BD Pharmingen
CD4	PE	1:400	eBioscience
CD19	BB700	1:400	BD Biosciences

Table 21: Lymphoid panel used for flow cytometric analysis of spleens and subcutaneous tumors

2.8. Statistical Analysis

All statistical tests are calculated using Graph Pad Prism 5.0 software and data are represented as mean ± standard deviation. Significance was assessed using Student's T-test or Mann- Whitney U test for two group comparison, while for comparisons involving more than two groups, two-way ANOVA or and one-way ANOVA with Turkey post-test was employed. Log rank test was used for Kaplan Meier survival analysis. For all tests, significance levels are defined as *p <0.05, ** p <0.01, *** p <0.001.

3. RESULTS

3.1. In vitro characterization of KPO cell line

To investigate the role of JAK1 and JAK2 in T-cell dependent LUAD, a tumor cell line was generated from KPO tumor bearing mouse model 10 weeks post tumor initiation. This experimental mouse model was established by crossing $KRAS^{LSL\text{-}G12D}$:$p53^{fl/fl}$ mice with mice harboring reversely oriented GFP-OVA construct, flanked by two sets of wt and mutant (L3) loxP sites, oriented in opposite direction. Subsequent inhalation of KPO mice with Cre-recombinase expressing adenovirus (Cre. Ad) triggers $KRAS^{G12D}$ mutation in lung epithelial cells, p53 deletion as well as expression of GFP-OVA fusion protein resulting in tumors recognized by T cells, and thus more closely resembling human LUAD (Figure 7A). OVA expression in this cell line was assessed by analyzing GFP expressing cells using flow cytometry as well as western blot analysis with GFP antibodies, and compared to the cell line that does not express GFP-OVA fusion protein (KP) (Figure 7B-C).

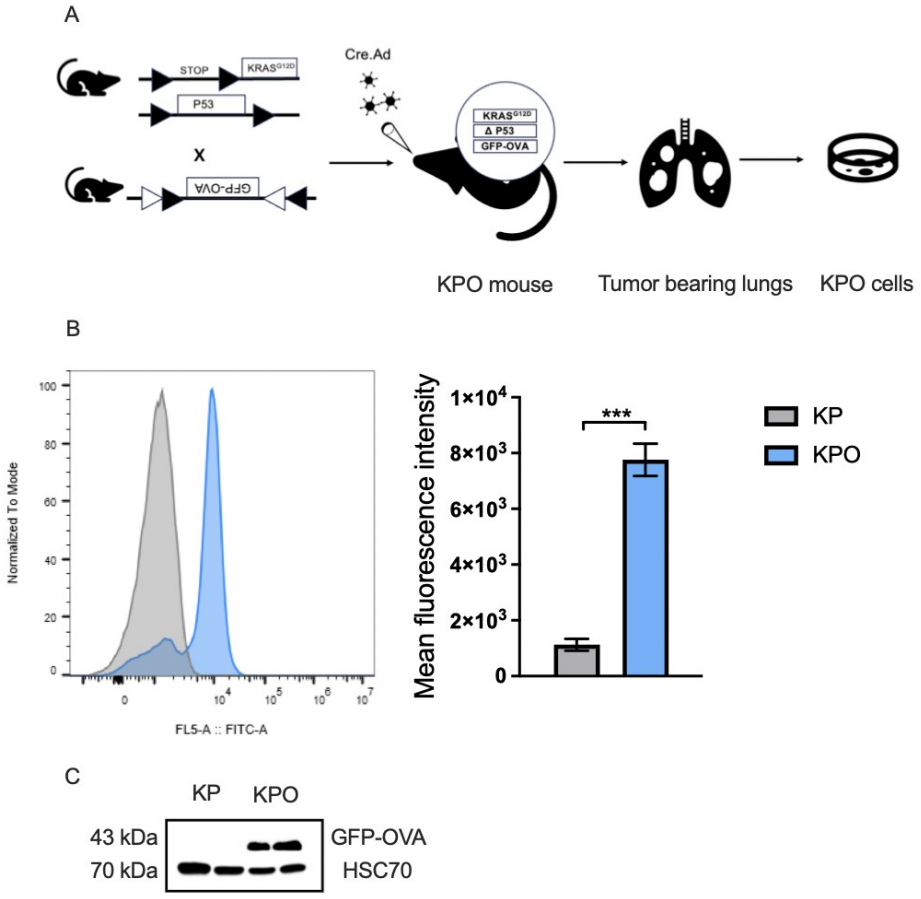

Figure 7: **KPO cell generation and assessment of OVA expression**. A) KPO cells isolated from tumor bearing KPO mouse, which was generated by crossing $KRAS^{LSL\text{-}G12D}$:$p53^{fl/f}$ mouse with mouse expressing GFP-OVA fusion protein. Black and white triangles represent loxPwt and mutant sites, respectively. B) Histogram illustrating fluorescence intensity of GFP-OVA in KPO cell line compared to KP cell line (left). Quantification of mean fluorescence intensity in KPO versus KP cell line (right). C) Expression of GFP-OVA protein in KPO cell line. B) T-test *p < 0.001

Next, in vitro T-cell killing assay was performed to further characterize KPO cell line and to assess T cell mediated tumor killing. Namely, $CD8^+$ T cells isolated from OT I mouse, which expresses transgenic T cell receptor designed to specifically recognize ovalbumin residues 265-264 in the context of MHC-I, were cocultured with KPO tumor cells. Following 5-day incubation, OT I T cells significantly reduced number of KPO colonies compared to KP colonies (Figure 8A-B).

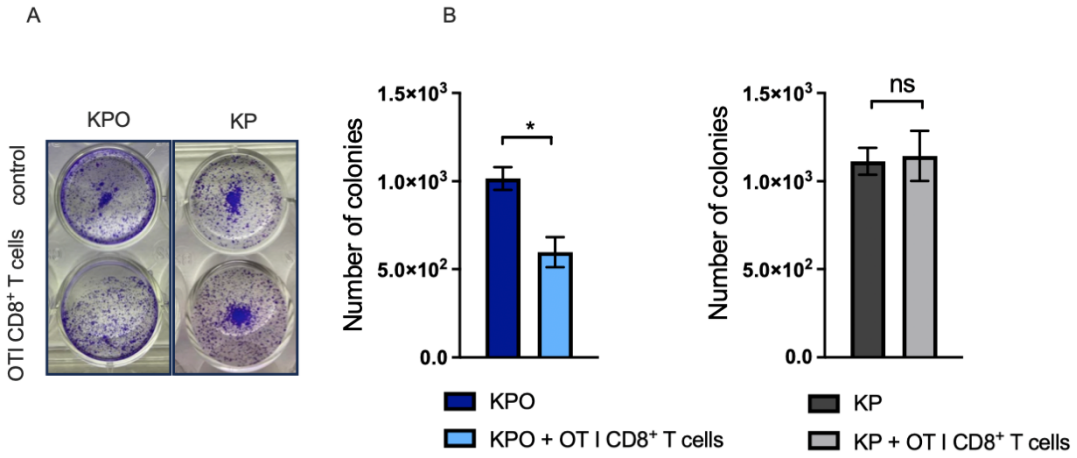

Figure 8: **In vitro T cell killing assay**. A) Colony formation assay upon coculture with OT I $CD8^+$ T cells. B) Quantitative analysis of colony formation. Mann Whitney U-Test *p <0.05

To mimic physiological conditions in which these cells typically function, involving local microenvironment and interaction between tumor cells and components of TME, KPO cells were treated with increasing concentrations of bronchoalveolar lavage (BAL) previously isolated from KPO mouse. Following treatment, tumor-derived cell expression of proinflammatory cytokine CXCL10 was significantly upregulated when treated with the highest BAL concentration accompanied by an increase in PD-L1 and MHC-I markers, which reached significance for PD-L1, as verified by real time quantitative PCR (Figure 9A-C). Since all these genes are IFNγ stimulated genes, KPO cells seem to exhibit IFNγ signature upon BAL stimulation.

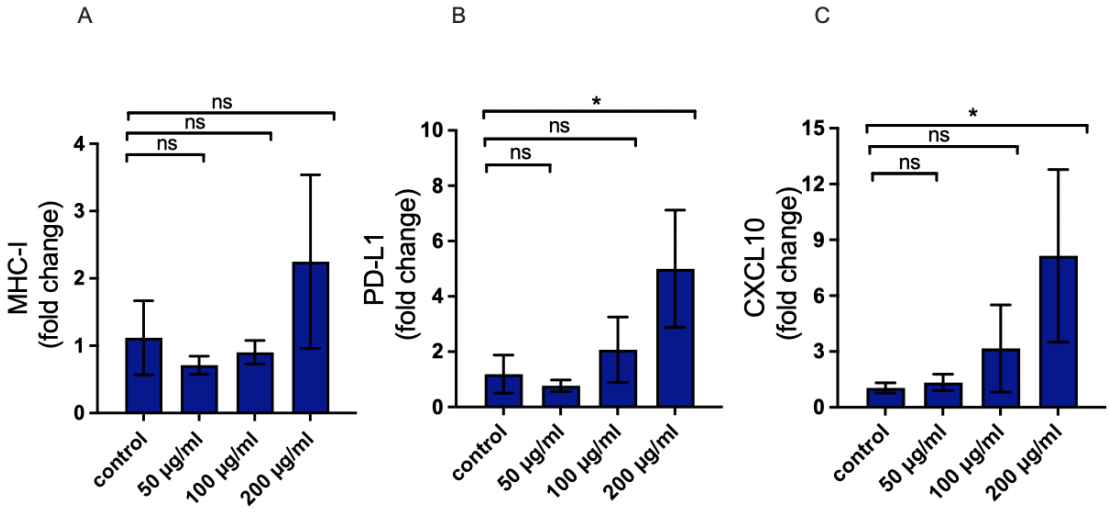

Figure 9: **KPO cells exhibit IFNγ signature upon BAL stimulation**. A-C) Real time quantitative PCR data showing MHC-I, PD-L1 and CXCL10, common IFNγ regulated genes, expression upon stimulation with increasing BAL concentrations retrieved from KPO mouse. A-C) One way ANOVA, *p <0.05

3.2. Systemic JAK1/2 inhibition with ruxolitinib promotes the growth of KPO cell line in vivo

To assess potential benefits of systemic JAK1/2 inhibition with ruxolitinib, KPO cell line was subcutaneously transplanted in immunocompetent C57BL6/N mice. Post tumor transplantation, mice were treated with ruxolitinib twice daily for 12 days. On the contrary to previously obtained results, ruxolitinib significantly promoted the growth of subcutaneous tumors as reflected by tumor volume and tumor weight at experimental endpoint (Figure 10B-D)

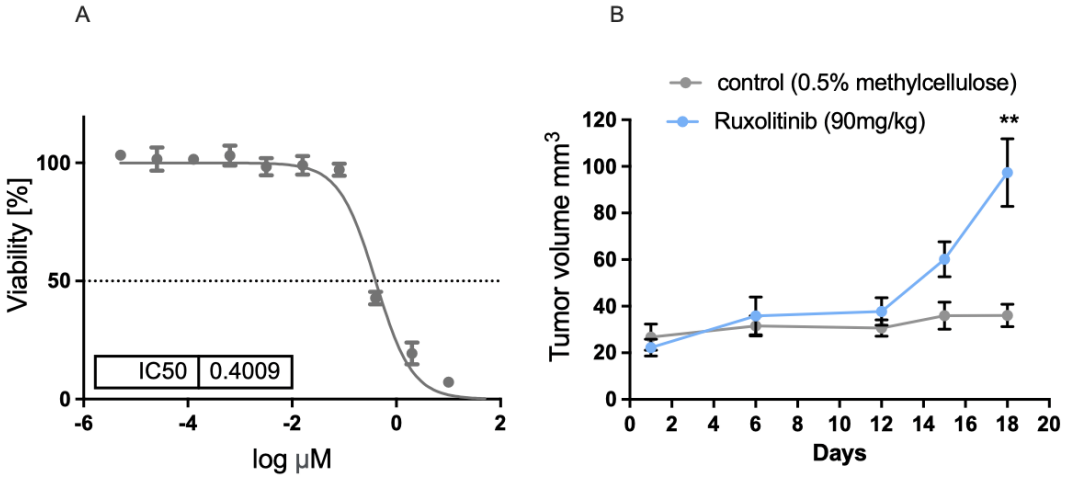

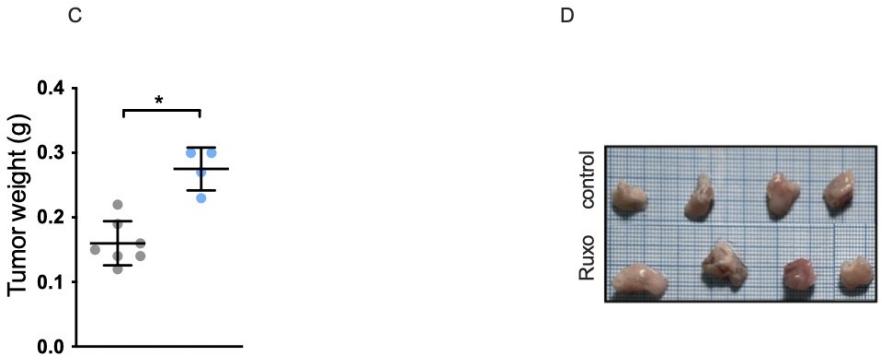

Figure 10: **Ruxolitinib promotes growth of subcutaneous tumors**. A) KPO cells respond to ruxolitinib in vitro (IC_{50}= 0.4μM*)*. B) Mean volumes of KPO subcutaneously transplanted tumors treated with 90mg/kg ruxolitinib or vehicle control twice daily. C) End point tumor weight. D) Representative pictures of KPO-derived tumors treated with ruxolitinib or vehicle control. B-C) Mann-Whitney U- test, *p<0.05, ** p<0.01. Data are represented as means ± SD.

Given the importance of JAK signaling in immune cell regulation and the reported immunosuppressive effects of ruxolitinib, coupled with increased tumor growth in ruxolitinib-treated group, the effect of JAK1/2 inhibition on TME was assessed. To do so, flow cytometric analysis of both, spleens and subcutaneous tumors was performed. In terms of lymphoid panel, there was a slight reduction in the abundance of $CD45^+CD3^+$, $CD45^+CD4^+$, $CD45^+CD8^+$ cells accompanied by an increase in $CD19^+$ B-cells in spleens of ruxolitinib-treated group (Figure 11A), however, no significant differences were observed. On the other hand, reduction of tumor infiltrating $CD3^+$, $CD4^+$ cells reached significance in ruxolitinib-treated group. Similar trend was observed for $CD8^+$ T cells, but the results were not significant (Figure 11B). These results highlight the influence of ruxolitinib on the microenvironment explaining increased tumor growth in ruxolitinib-treated group by impaired immune system.

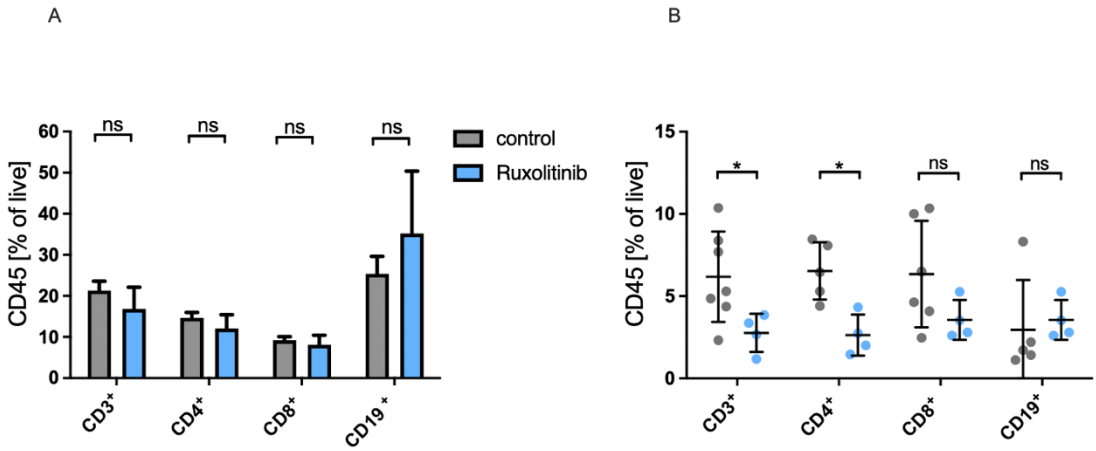

Figure 11: **JAK inhibition impairs immune system leading to tumor progression.** A-B) Flow cytometric analysis showing the percentage of lymphoid cells in ruxolitinib-treated group or vehicle control in spleens (left) and subcutaneous tumors (right). Mann-Whitney *U*- test, *p<0.05, ** p<0.01. Data are represented as means ± SD.

3.3. Establishing KPO knockout cell lines using CRISPR-Cas9 technology

Having shown that systemic JAK1/2 inhibition with ruxolitinib positively influences progression of subcutaneously transplanted KPO tumors, we next wanted to determine whether this influence was a result of direct or indirect effect of microenvironment. Furthermore, under physiological conditions, the actual tumor cells exhibited induction of IFNγ stimulated genes, known to engage JAK1 and JAK2 to transmit signals. Thus, the effect of JAK inhibition only in tumor cells was assessed by employing CRISPR/Cas9 technology to produce KPO JAK1, JAK2 and JAK1/2 knockout (KO) cells, namely, KPO $^{\Delta JAK1}$, KPO $^{\Delta JAK2}$ and KPO $^{\Delta JAK1/2}$ cell lines. After generation of single clones for each cell line, KOs were firstly verified by TIDE (Tracking of Indels by Decomposition) method, which estimates spectrum and frequency of insertions and deletions (indels) using Sanger sequencing. Results were analyzed using TIDE web tool (Figure 12 A-B). JAK1 KO was accomplished by a single nucleotide insertion, JAK2 by inserting and deleting one nucleotide in the proximity of the expected break site, whereas double knockout resulted from a deletion of a single nucleotide in the case of JAK1 KO, and deletion and insertion of one nucleotide in the case of JAK2 (Figure 12C-E). All generated clones had a KO efficiency >95%.

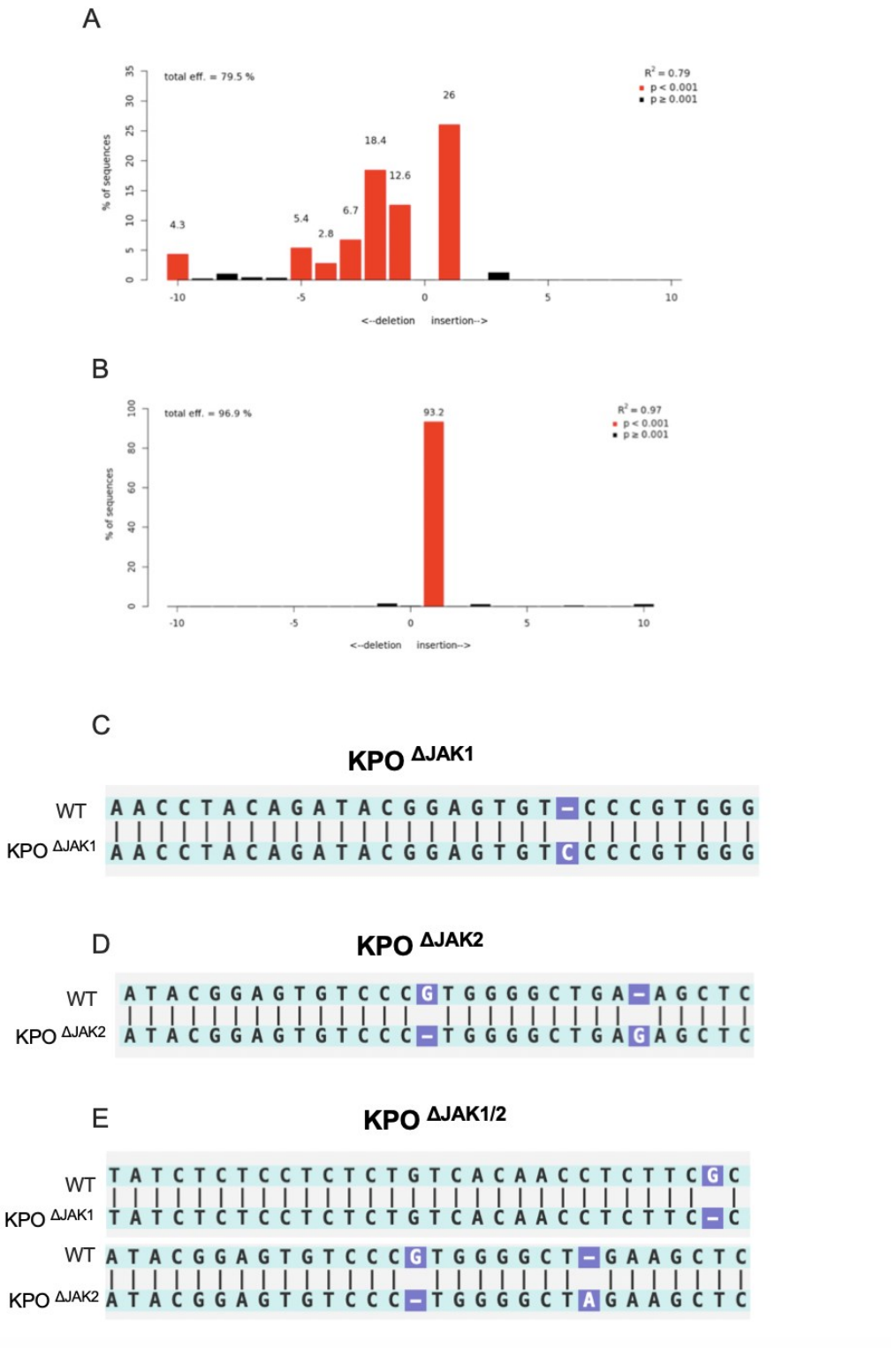

Figure 12: **Assessment of genome editing using TIDE**. A) Example of a profile of all indels within pool of cells. B) Example of a single clone achieved through an insertion of a single nucleotide. C) Pairwise sequence alignment of WT and KPO$^{\Delta JAK1}$ D) WT and KPO$^{\Delta JAK2}$ and E) WT and KPO$^{\Delta JAK1/2}$. R^2 represents a coefficient of determination. C-D) Created using Vector Builder's Sequence Alignment Tool (www.vectorbuilder.com).

Decreased mRNA levels of the JAKs were observed in the KO cell lines as determined by real time quantitative PCR (Figure 13A-B). Likewise, KOs were confirmed in western blot analysis (Figure 13C).

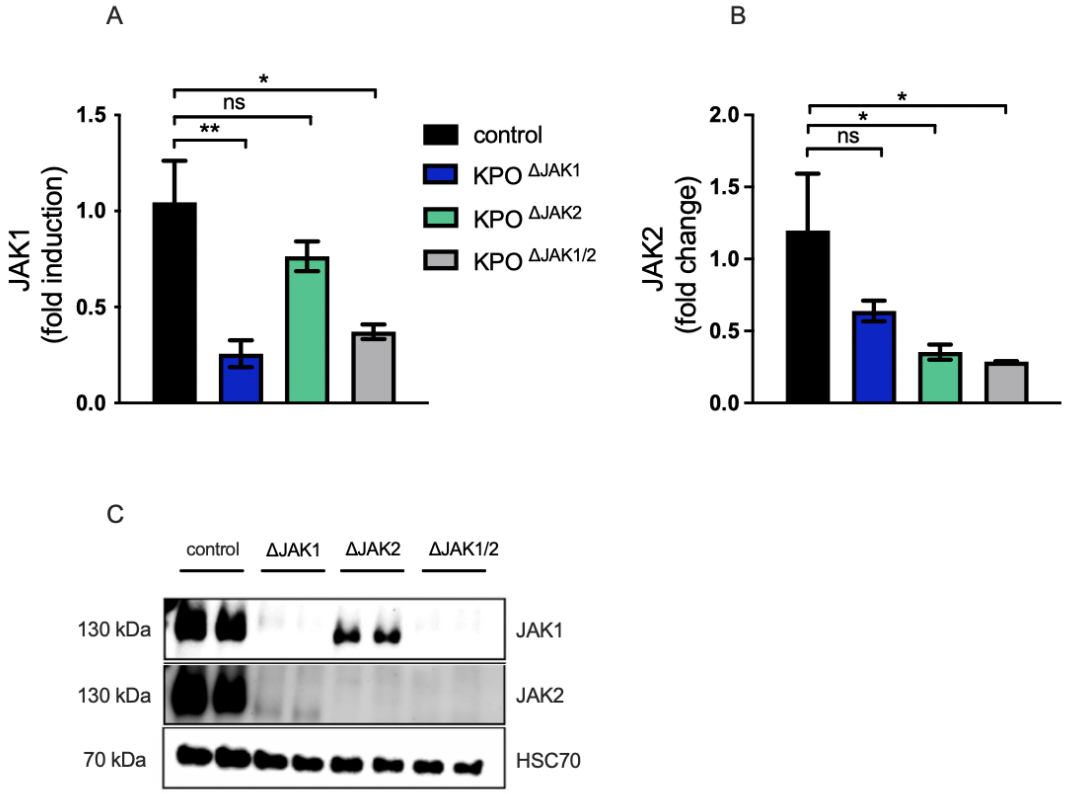

Figure 13: **Knockout validation**. A) mRNA expression levels of JAK1 B) JAK2 as determined by real time quantitative PCR. B) Western blot analysis for JAK1 and JAK2 using HSC70 as loading control. A-B) Two-way ANOVA, *p<0.05

3.4. IFNγ signaling is abrogated in KPO$^{\Delta JAK}$ cell lines

Following successful generation of KO cell lines using KPO cells, which demonstrated IFNγ signature under physiological conditions, expression of target genes and downstream effectors was investigated. Specifically, we investigated expression of genes that appeared to be upregulated after BAL stimulation. While untreated cells express basal levels of MHC-I and PD-L1, upon IFNγ stimulation KO cell lines exhibited a significant decrease in the expression of both markers on the mRNA as well as protein level when compared to control cells (Figure 14A, C). Moreover, the downstream signaling targets of JAKs, namely phosphorylated STAT1 and STAT3 could not be detected at the protein level in the KO cells when stimulated with IFNγ. Some levels of pSTAT3 could, however, be detected in JAK2 KO. This contrasts with treated control cells providing a functional conformation of the KOs (Figure 14B).

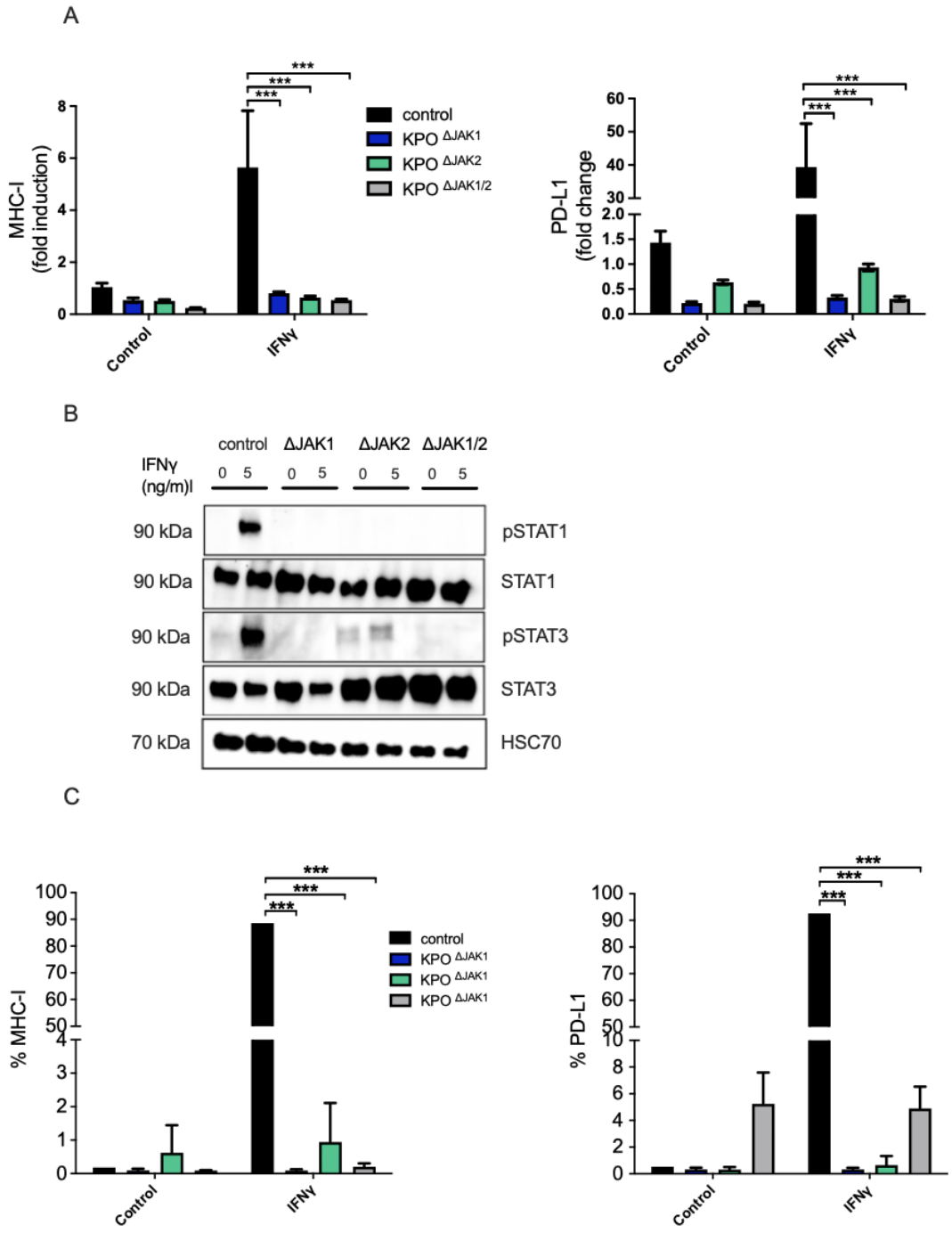

Figure 14: **IFNγ signaling in JAK KO cell lines**. A) mRNA expression levels of MHC-I (left) and PD-L1 (right) upon 5 ng/ml IFNγ stimulation as determined by real time quantitative PCR. B) Western blot analysis of JAK downstream targets, pSTAT1 and pSTAT3, upon stimulation. C) Flow cytometric analysis of cell surface markers, MHC-I and PD-L1. A, C) Two way ANOVA, *p<0.05

3.5. Tumor intrinsic JAK deletion fails to slow growth of subcutaneous tumors

Given that systemic inhibition of JAK1/2 in T-cell dependent experimental model promoted progression of KRAS-driven LUAD, next we wanted to assess tumor cell intrinsic effects of JAK1/2 deletion in vivo. Thus, KPO and KPO$^{\Delta JAK1/2}$ cells were transplanted subcutaneously in immunocompetent C57BL6/N mice and tumor growth was observed within 3 weeks. Interestingly, no significant differences were observed between two experimental groups with KPO $^{\Delta JAK1/2}$ tumors exhibiting slightly accelerated growth (Figure 15A-B). KPO cells did not show growth advantage over KO cells in vivo.

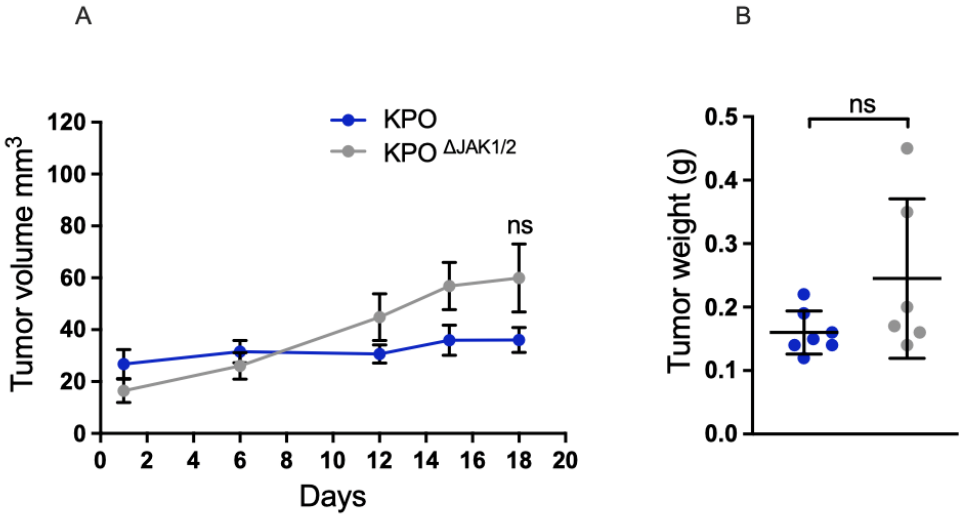

Figure 15: **Subcutaneous engraftment of KPO and KPO$^{\Delta JAK1/2}$ cells in immunocompetent C57BL6/N mice.** A) Mean volumes of KPO and KPO$^{\Delta JAK1/2}$ transplanted tumors. B) Tumor weight at the conclusion of the experiment.

Moreover, the effect of ruxolitinib was also assessed in KPO$^{\Delta JAK1/2}$ subcutaneously transplanted tumors to examine its effect solely in immune cells, considering that KPO$^{\Delta JAK1/2}$ should be insensitive to the treatment. As previously described, mice were treated with 90 mg/kg ruxolitinib or vehicle control twice daily for 2 weeks. At the endpoint, subcutaneous tumors were excised, weighed and immune cell infiltration was examined using flow cytometry. Likewise, spleens were isolated and subjected to analysis. Treatment significantly increased growth of KPO$^{\Delta JAK1/2}$ transplanted cells (Figure 16A-C). The obtained results align with our prior observations. Even though spleen weight did not differ between two experimental groups, there were significantly reduced numbers of CD45$^+$CD3$^+$ as well as CD45$^+$CD4$^+$ in the spleens of ruxolitinib-treated mice (Figure 16D). In the case of subcutaneous tumor infiltration, there was significant decrease in CD8$^+$ T cells in addition to previously observed significantly reduced number of CD45$^+$CD3$^+$ and CD45$^+$CD4$^+$ T cells (Figure 16E).

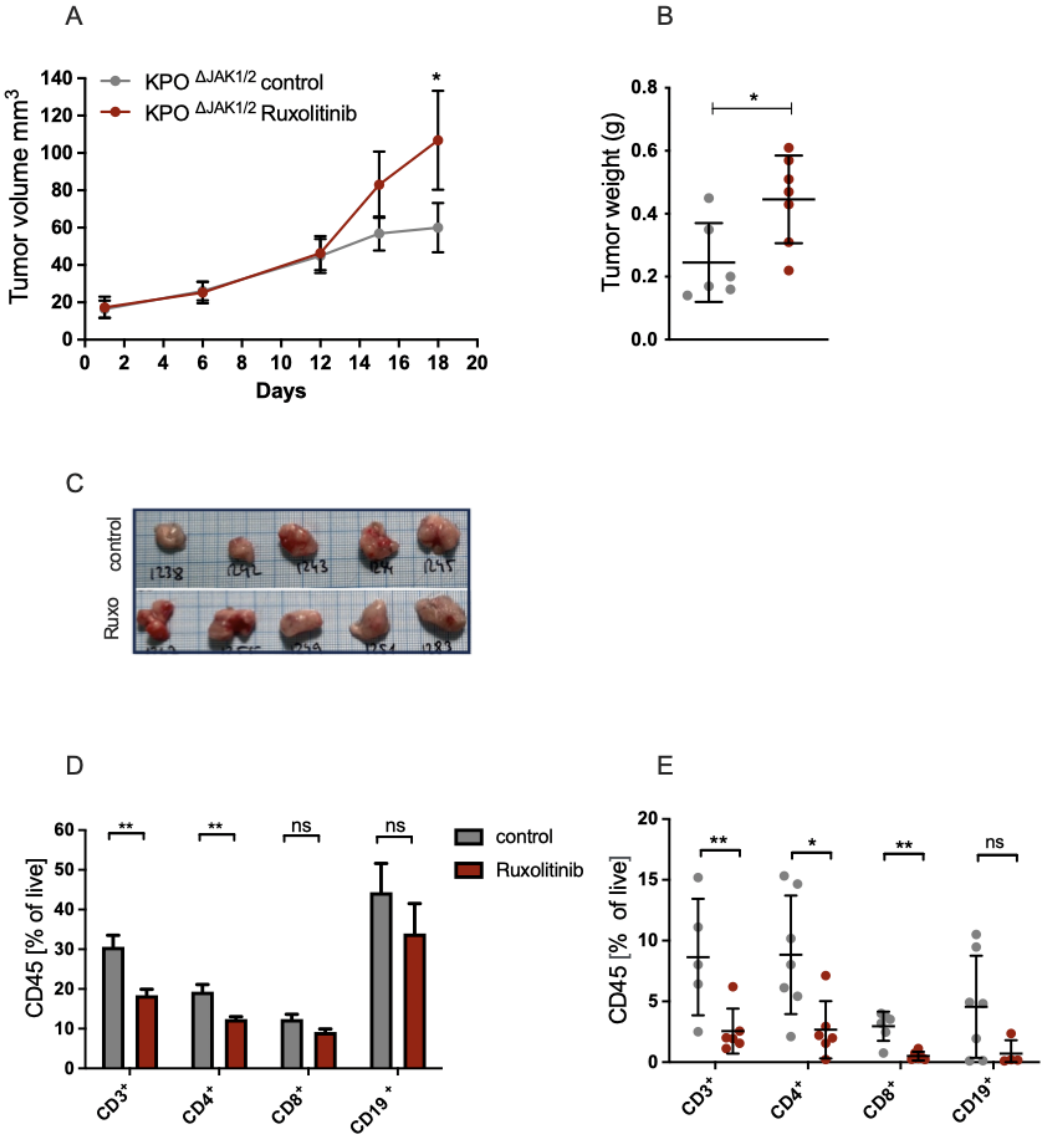

Figure 16: **Effect of ruxolitinib on KPO$^{\Delta JAK1/2}$ subcutaneous tumors**. A) Mean tumor volume of KPO$^{\Delta JAK1/2}$ subcutaneous tumors in immunocompetent C57BL6/N mice treated with 90 mg/kg ruxolitinib or vehicle control twice daily. B) Tumor weight upon experiment conclusion. C) Representative pictures of subcutaneous tumors in the treatment and control group. D) Flow cytometric analysis showing the percentage of lymphoid cells in ruxolitinib-treated group or vehicle control in spleens (left) and subcutaneous tumors (right). A-B, D-E) Mann-Whitney *U*- test, *p<0.05, ** p<0.01. Data are represented as means ± SD.

Intratracheal transplantation of JAK KO cells leads to reduced survival of only KPO$^{\Delta JAK2}$ recipients

While subcutaneous tumors offer easy accessibility, monitoring and drug response assessment, this experimental model might not be optimal in the case of lung cancer. It is important to consider that the observed results and treatment responses in subcutaneous tumors may not entirely mirror the complexity of lung cancer in its natural environment. Therefore, single JAK KO cell lines, namely KPO$^{\Delta JAK1}$ and KPO$^{\Delta JAK2}$ were transplanted intratracheally into immunocompetent C57BL6/N mice. An orthotopic model like this better captures tumor development and progression. In vitro proliferation assay of single JAK KO cell lines showed significantly increased proliferation of KPO $^{\Delta JAK1}$ when compared to KPO$^{\Delta JAK2}$ or control cells (Figure 17 A) . While all three cell lines engrafted successfully and were able to form tumors, transplantation led to significantly decreased survival of only those mice that received KPO$^{\Delta JAK2}$ cell line (Figure 17B-D).

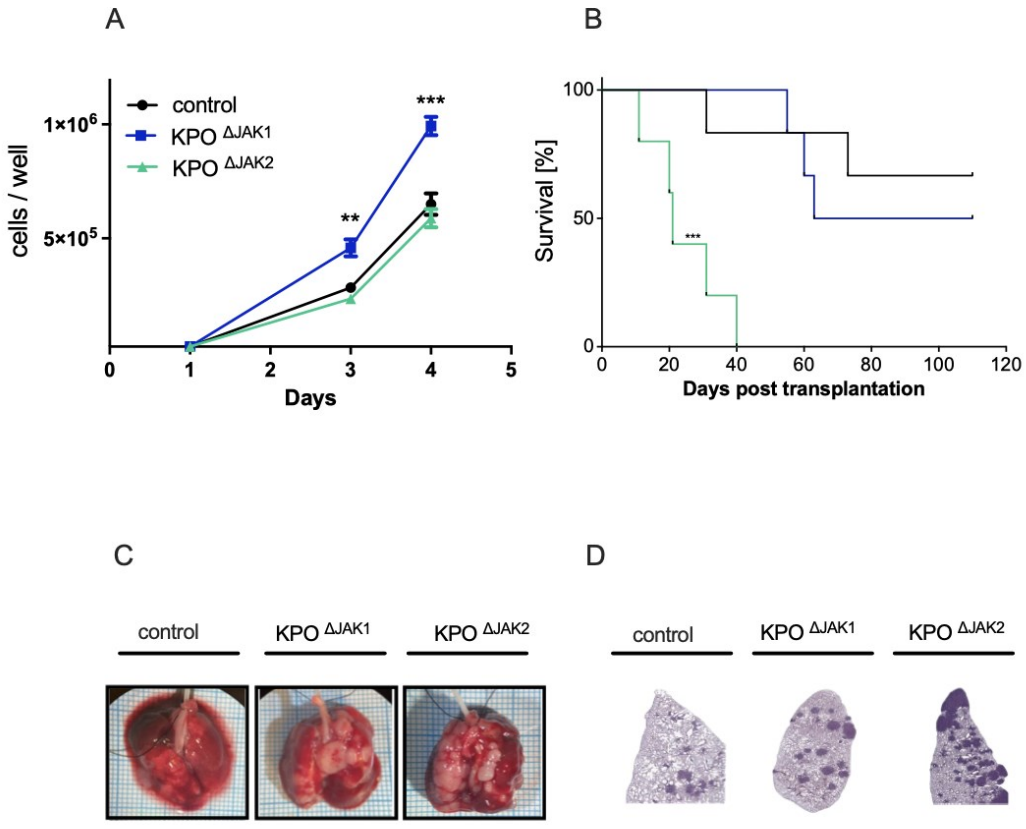

Figure 17: **Orthotopic transplantation of KPO$^{\Delta JAK1}$ and KPO$^{\Delta JAK2}$ in immunocompetent C57BL6/N mice.** A) In vitro proliferation assay B) Kaplan-Meier analysis of intratracheally transplanted KPO (n=5), KPO$^{\Delta JAK1}$ (n=5), KPO$^{\Delta JAK2}$ (n=5) cell lines. C) Representative pictures of isolated lungs. D) Representative pictures of H&E staining. A)Two-way ANOVA ** $p<0.01$ B) Log-rank test *** $p<0.001$

4. DISCUSSION

Despite the progress in lung cancer research, lung cancer remains the most common cause of cancer related mortality globally. High molecular heterogeneity of lung cancer contributes to drug resistance, demanding the use of combination therapies (Zito Marino et al., 2019). Unfortunately, individuals with KRAS-mutated LUAD exhibit limited responsiveness to all current therapeutic approaches, highlighting the importance of developing novel therapeutic strategies. Since the progression of KRAS-mutated LUAD has been closely linked with inflammation, JAKs, as a core molecules in inflammation present a focus for therapeutic intervention. As shown and reported by Mohrherr et al., JAK1/2 inhibition attenuated the growth of KRAS-mutated LUAD experimental model by reshaping TME towards anti-inflammatory and anti-tumorigenic. Notably, JAK inhibition led to a decrease in the number of tumor infiltrating $CD4^+$ and $CD8^+$ T cells as well as NK cells, however, it also abrogated IFNγ mediated STAT1 signaling reducing PD-L1 expression. While this study suggests beneficial role of JAK1/2 inhibition on tumorigenesis of KRAS-mutated LUAD, it is important to emphasize that T cells have a limited impact in the used experimental mouse model, and it is therefore hard to deduce whether immunosuppressive role of JAK inhibition would prevail its antitumorigenic effects and allow tumor development. Thus, the aim of this thesis was to investigate the role of JAKs in T-cell dependent experimental model of KRAS-mutated LUAD.

4.1. Systemic JAK1/2 inhibition does not slow the growth of subcutaneous tumors

To explore the role of JAKs in T-cell dependent model, we took advantage of KPO cell line, which not only harbors the $KRAS^{G12D}$ mutation and p53 deletion, but it also expresses highly immunogenic ovalbumin protein, resulting in tumors infiltrated by T cells. Our results demonstrate that systemic inhibition of JAK1/2 with ruxolitinib does not slow tumor growth as previously demonstrated in T-cell independent experimental model. On the contrary, growth of subcutaneous KPO tumors transplanted in C57BL6/N mice was significantly increased upon treatment with ruxolitinib, as demonstrated by tumor volume and weight upon conclusion of the experiment (Figure 10A-D). Flow cytometric analysis of subcutaneous tumors revealed reduction in immune cell infiltration in the tumors, which reached significance for total $CD3^+$ and $CD4^+$ T cells (Figure 11B). In line with this data, Mohrherr et al. also demonstrated that ruxolitinib treatment results in immunosuppression, as shown by reduced numbers of tumor infiltrating $CD4^+$ and $CD8^+$ T cells, as well as of NK cells. Different studies have confirmed immune suppressive role of JAK inhibition which led to increased tumor burden (Curran et al., 2017; Bottos et al., 2016). Given that ruxolitinib is known to act on various components of both, innate and adaptive immune system, and considering the complexity of the pathways governed by JAK1 and JAK2, it is likely that ruxolitinib has numerous additional cellular targets

(Elli et al., 2019). Moreover, significance of assessing ruxolitinib treatment in T-cell dependent experimental model lies in understanding its potential impact on standard of care for KRAS mutated LUAD patients, which is immunotherapy. Since immunotherapy stimulates immune system to recognize and attack cancer cells, immunosuppressive agent like ruxolitinib could counteract potential benefits of immunotherapy and limit effectiveness of the treatment. However, use of anti-inflammatory and immunosuppressive drugs presents a dual challenge. While anti-inflammatory drugs weaken immune system and thus promote tumorigenesis, they can also be beneficial by reducing chronic inflammation, which is associated with increased risk of cancer. For instance, IL1ß, a key mediator of inflammatory response primarily produced by monocytes, macrophages and dendritic cells, has been implicated in promoting lung cancer tumorigenesis and metastasis. Its role in tumorigenesis is partly attributed to its effect on immune cells, such as macrophage polarization towards M2 phenotype and its association with high percentage of MDSCs. In this context, inhibiting IL1ß to reduce inflammation would be beneficial in lung cancer (Garon, Chih-Hsin Yang and Dubinett, 2020; Zhang and Veeramachaneni, 2022). Nevertheless, our results suggest that suppressing inflammation by systemically targeting JAKs in KRAS-mutated LUAD does not appear to confer a beneficial effect on tumorigenesis.

4.2. KPO cells display characteristic of IFNγ activation under physiological conditions

To further characterize KPO cells and their interaction with microenvironment, cells were stimulated with bronchoalveolar lavage collected from KPO mouse. Stimulation led to increased expression of IFNγ induced genes as demonstrated by expression levels of MHC-I, PD-L1 as well as CXCL10 (Figure 9A-C). Despite its tumor growth inhibitory capabilities, prolonged exposure to IFNγ may also foster tumor development (Mojic, Takeda and Hayakawa, 2017). This extended exposure has been shown to trigger the synthesis of PD-L1, an immune checkpoint inhibitory molecule as well as indoleamine-2,3-dioxygenase (IDO), thereby activating immunosuppressive mechanisms. Consequently, this results in suppressing T cell activity in a number of different tumors including NSCLC (Jorgovanovic et al., 2020; Zhang et al., 2017). IFNγ exerts its biological effects by activating intracellular molecular signaling pathways, mainly through JAK/STAT signaling pathway (Castro et al., 2018). Given the context, establishing JAK KOs in tumor cells has emerged as a prospective strategy to investigate JAKs specific role within tumor microenvironment. Using CRISPR/Cas9 technology, single JAK KOs, $KPO^{\Delta JAK1}$ and $KPO^{\Delta JAK2}$, as well as double $KPO^{\Delta JAK1/2}$ KO were established. As expected, disruption of JAK1 and JAK2 resulted in decreased expression of genes stimulated by IFNγ, as demonstrated by the levels of MHC-I and PD-L1 in KO cell lines

as well as levels of phosphorylated STAT1 and STAT3 (Figure 14A-C). While JAK1 KO resulted in a complete loss of pSTAT3 expression, modest presence of pSTAT3 was detected in JAK2 KO samples (Figure 14B). These findings suggest a potential compensatory role of JAK1, as its expression might partially compensate for the loss of JAK2.

4.3. Intrinsic JAK deletion does not slow growth of subcutaneous tumors, however orthotopic transplantation leads to decreased survival of only KPO$^{\Delta JAK2}$ recipients

Since systemic JAK inhibition with ruxolitinib increased growth of KPO subcutaneous tumors due to reduced infiltration of immune cells in the tumors, intrinsic JAK deletion was assessed next. Interestingly, subcutaneously transplanted KPO cells did not have a growth advantage over double JAK1/2 KO (Figure 15A-B). These findings suggest that alternative pathways allow for sustained growth and compensate for the loss of JAK1/2 signaling or that JAK1/2 may be dispensable in this experimental model. It is important to consider intricate interplay between signaling pathways and the potential combinatorial approaches that could influence tumorigenesis. In the context of lung cancer, signaling pathways interconnected with JAK/STAT signaling such as RAS/MAP/ERK as well as PI3K/Akt/STAT3/NF-κB also play an important role in NSCLC (Hasan et al., 2023). For instance, efficacy of therapy has been shown to be influenced by the modulation of cytokine responses through MEK inhibition (Xie et al., 2019). In untreated tumors, elevated JAK1/STAT3 signaling was linked to a higher expression of AXL, a molecule implicated in various pathways associated with cell proliferation, migration, and invasion. Thus, a potential novel therapeutic approach in lung cancer was suggested that would combine AXL and JAK1 inhibition (Taverna et al., 2020). This highlights the importance of considering potential compensatory mechanisms within the signaling network, where impact of a particular pathway may only become pronounced when other crucial compensating pathways are affected as well.

Moreover, subcutaneously transplanted KPO$^{\Delta JAK1/2}$ tumors subjected to ruxolitinib treatment exhibited tumor growth advantage upon treatment (Figure 16A-C). Consistent with previous findings, ruxolitinib significantly diminished tumor infiltrating CD4$^+$ and CD8$^+$ T cells (Figure 16E). Since KPO$^{\Delta JAK1/2}$ tumors are insensitive to the ruxolitinib treatment, this further confirms the importance of ruxolitinib's impact on the immune system rather than on the tumor cells in this experimental model.

However, one of the major drawbacks of subcutaneous tumors when studying lung cancer is that they do not accurately mimic the lung environment. Intratracheal transplantation, on the other hand, allows direct introduction of cancer cells in the lungs representing natural conditions in which lung tumors develop and progress. Thus, orthotopic transplantation of single KOs, KPO$^{\Delta JAK1}$ and KPO$^{\Delta JAK2}$, was performed. While all cell lines successfully engrafted

in immunocompetent mice and were able to form tumors, significantly decreased survival was only observed in the recipients of KPO$^{\Delta JAK2}$ cell line (Figure 17B). On the contrary, KPO$^{\Delta JAK1}$ cell line showed significantly increased proliferation in vitro compared to other KO cell lines and control, underscoring the importance of TME on tumor progression (Figure 17A). Thus, these results suggest tumor intrinsic effect of JAK2 in the orthotopic experimental model. Nevertheless, it is hard to deduce from this model whether the loss of JAK2 would be compensated by JAK1. In agreement with previous reports, presence of JAK1 was shown to partially compensate for JAK2 signaling as demonstrated by phosphorylation of STAT3 (Majoros et al., 2017). This contrasts with JAK1 deficient cells, where JAK2 failed to compensate for the absence of JAK1 (Witalisz-Siepracka et al., 2019). For a better understanding of potential compensatory effects of JAK1 and JAK2 in tumor cells, it is crucial to repeat intratracheal transplantation experiment with KPO cell line lacking both, JAK1 and JAK2. Moreover, use of JAK1/2 deficient genetically engineered lung cancer mouse model would offer a better perspective. Interestingly, according to TCGA PanCancer Atlas data of KRAS-mutated LUAD, patients with higher expression of JAK2 had longer overall survival compared to patients with lower JAK2 expression levels, which suggests potential beneficial role of JAK2 in prolonging survival. Yet, the precise mechanisms underlying the specific role of JAK2 in this context remain to be elucidated.

5. CONLUSION AND OUTLOOK

Here, we demonstrate that systemic JAK1/2 inhibition with ruxolitinib enhances growth of subcutaneous tumors in the T-cell dependent experimental model of KRAS-driven LUAD. Additionally, ruxolitinib has exhibited a greater effect on immune cells compared to tumor cells, as evidenced by the increased tumor growth in JAK1/2 KO cell line. Namely, treatment results in downregulation of tumor infiltrating helper CD4$^+$ and cytotoxic CD8$^+$ T cells, thereby compromising immune surveillance and facilitating tumor growth. Taking this into account, combining JAK inhibitors or other immunosuppressive drugs with immunotherapy does not seem to be beneficial in this experimental model of the KRAS-driven LUAD. However, to validate these finding and further explore the effects of JAKs in the T-cell dependent experimental model, rather than a transplant model, it is crucial to assess ruxolitinib treatment in genetically engineered KPO mouse model at both, early and late stages of tumor induction. This approach allows for an assessment of how ruxolitinib affects progression of already established KRAS-driven LUAD in therapeutic setting. Importantly, genetically engineered mouse more closely resembles genetic complexity and heterogeneity of human tumors, and thus enhances translational relevance of the findings (Kersten et al., 2016).

On the other hand, intrinsic JAK1/2 deletion in tumor cells abrogates IFNγ signaling, as demonstrated by reduced PD-L1 and MHC-I expression levels, however, it fails to slow the growth of subcutaneous tumors. These results imply that JAK1/2 signaling might not be essential in this experimental model or that alternative pathways may facilitate continued growth. Interestingly, intratracheal transplantation of single JAK KOs has led to a decreased survival of only those mice that received $KPO^{\Delta JAK2}$ cell line. To investigate possible compensatory effect, intratracheal instillation with double JAK KO would provide a better insight into interplay between JAK1 and JAK2 signaling. The underlying mechanisms of the role that JAK2 has in tumor cells are yet to be elucidated. Characterization of immune cell infiltrates in the tumors established with single as well as double JAK knockouts would provide further insights in the importance of different cell types in KRAS tumorigenesis. Moreover, to comprehensively investigate changes in signaling pathways resulting from JAK KOs, phosphoproteomics analysis could be employed. By comparing phosphoproteomics profiles of different KO, novel signaling targets can be identified that might hold therapeutic significance and could potentially be integrated in combination therapies thereby improving response to KRAS-driven LUAD.

To conclude, combination of anti-inflammatory and immunosuppressive drugs with immunotherapy, the standard treatment for KRAS-driven LUAD, does not impair tumor progression. Additionally, JAK2 appears to play a significant role in the tumor cells in orthotopic transplantation model, however, specific mechanisms underlying its involvement remain to be fully understood.

6. References

1. Abubaker, K., Luwor, R.B., Zhu, H., McNally, O., Quinn, M.A., Burns, C.J., Thompson, E.W., Findlay, J.K. and Ahmed, N. (2014). Inhibition of the JAK2/STAT3 pathway in ovarian cancer results in the loss of cancer stem cell-like characteristics and a reduced tumor burden. *BMC Cancer*, 14(1). doi:https://doi.org/10.1186/1471-2407-14-317.
2. Ahrendt, S.A., Decker, P.A., Alawi, E.A., Zhu, Y., Sanchez-Cespedes, M., Yang, S.C., Haasler, G.B., Kajdacsy-Balla, A., Demeure, M.J. and Sidransky, D. (2001). Cigarette smoking is strongly associated with mutation of the K-ras gene in patients with primary adenocarcinoma of the lung. *Cancer*, 92(6), pp.1525–1530. doi:https://doi.org/10.1002/1097-0142(20010915)92:6%3C1525::aid-cncr1478%3E3.0.co;2-h.
3. Amanam, I., Mambetsariev, I., Gupta, R., Achuthan, S., Wang, Y., Pharaon, R., Massarelli, E., Koczywas, M., Reckamp, K. and Salgia, R. (2020). Role of immunotherapy and co-mutations on KRAS-mutant non- small cell lung cancer survival. *Journal of Thoracic Disease*, [online] 12(9). doi:https://doi.org/10.21037/jtd.2020.04.18.
4. Arulogun, S.O., Choong, H.-L., Taylor, D., Ambrosoli, P., Magor, G., Irving, I.M., Keng, T.-B. and Perkins, A.C. (2017). JAK1 somatic mutation in a myeloproliferative neoplasm. *Haematologica*, [online] 102(8), pp.e324–e327. doi:https://doi.org/10.3324/haematol.2017.170266.
5. Babar, L., Raj, M.S. and Anjum, F. (2020). *Lung Cancer Screening*. [online] PubMed. Available at: https://www.ncbi.nlm.nih.gov/books/NBK537283/.
6. Banerjee, S., Biehl, A., Gadina, M., Hasni, S. and Schwartz, D.M. (2017). JAK–STAT Signaling as a Target for Inflammatory and Autoimmune Diseases: Current and Future Prospects. *Drugs*, 77(5), pp.521–546. doi:https://doi.org/10.1007/s40265-017-0701-9.
7. Beinhoff, P., Sabharwal, L., Vindhya Udhane, Maranto, C., LaViolette, P.S., Jacobsohn, K., Tsai, S., Iczkowski, K.A., Wang, L., Hall, W.A., Dehm, S.M., Deepak Kilari and Nevalainen, M.T. (2021). Second-Generation Jak2 Inhibitors for Advanced Prostate Cancer: Are We Ready for Clinical Development? *Cancers*, 13(20), pp.5204–5204. doi:https://doi.org/10.3390/cancers13205204.
8. Bharadwaj, U., Kasembeli, M.M., Robinson, P. and Tweardy, D.J. (2020). Targeting Janus Kinases and Signal Transducer and Activator of Transcription 3 To Treat Inflammation, Fibrosis, and Cancer: Rationale, Progress, and Caution. *Pharmacological Reviews*, [online] 72(2), pp.486–526. doi:https://doi.org/10.1124/pr.119.018440.
9. Bottos, A., Gotthardt, D., Jason M.R. Gill, Albana Gattelli, Frei, A., Alexandar Tzankov, Sexl, V., Aleksandra Wodnar-Filipowicz and Hynes, N.E. (2016). Decreased NK-cell tumour immunosurveillance consequent to JAK inhibition enhances metastasis in breast cancer models. *Nature Communications*, 7(1). doi:https://doi.org/10.1038/ncomms12258.
10. Bray, F., Laversanne, M., Weiderpass, E. and Soerjomataram, I. (2021). The ever-increasing importance of cancer as a leading cause of premature death worldwide. *Cancer*, 127(16). doi:https://doi.org/10.1002/cncr.33587.
11. Brenner, D.R., Boffetta, P., Duell, E.J., Bickeboller, H., Rosenberger, A., McCormack, V., Muscat, J.E., Yang, P., Wichmann, H. - E., Brueske-Hohlfeld, I., Schwartz, A.G., Cote, M.L., Tjonneland, A., Friis, S., Le Marchand, L., Zhang, Z.-F. ., Morgenstern, H., Szeszenia-Dabrowska, N., Lissowska, J. and Zaridze, D. (2012). Previous Lung

Diseases and Lung Cancer Risk: A Pooled Analysis From the International Lung Cancer Consortium. *American Journal of Epidemiology*, 176(7), pp.573–585. doi:https://doi.org/10.1093/aje/kws151.

12. Brooks, G.D., McLeod, L., Alhayyani, S., Miller, A., Russell, P.A., Ferlin, W., Rose-John, S., Ruwanpura, S. and Jenkins, B.J. (2016). IL6 Trans-signaling Promotes KRAS-Driven Lung Carcinogenesis. *Cancer Research*, [online] 76(4), pp.866–876. doi:https://doi.org/10.1158/0008-5472.CAN-15-2388.
13. Calles, A., Liao, X., Sholl, L.M., Rodig, S.J., Freeman, G.J., Mohit Butaney, Lydon, C.A., Dahlberg, S.E., F. Stephen Hodi, Oxnard, G.R., Jackman, D.M. and Jänne, P.A. (2015). Expression of PD-1 and Its Ligands, PD-L1 and PD-L2, in Smokers and Never Smokers with KRAS-Mutant Lung Cancer. 10(12), pp.1726–1735. doi:https://doi.org/10.1097/jto.0000000000000687.
14. Campbell, J.D., Alexandrov, A., Kim, J., Wala, J., Berger, A.H., Pedamallu, C.S., Shukla, S.A., Guo, G., Brooks, A.N., Murray, B.A., Imielinski, M., Hu, X., Ling, S., Akbani, R., Rosenberg, M., Cibulskis, C., Ramachandran, A., Collisson, E.A., Kwiatkowski, D.J. and Lawrence, M.S. (2016). Distinct patterns of somatic genome alterations in lung adenocarcinomas and squamous cell carcinomas. *Nature Genetics*, [online] 48(6), pp.607–616. doi:https://doi.org/10.1038/ng.3564.
15. Castro, F., Cardoso, A.P., Gonçalves, R.M., Serre, K. and Oliveira, M.J. (2018). Interferon-Gamma at the Crossroads of Tumor Immune Surveillance or Evasion. *Frontiers in Immunology*, 9(847). doi:https://doi.org/10.3389/fimmu.2018.00847.
16. Chevallier, M., Borgeaud, M., Addeo, A. and Friedlaender, A. (2021). Oncogenic driver mutations in non-small cell lung cancer: Past, present and future. *World Journal of Clinical Oncology*, [online] 12(4), pp.217–237. doi:https://doi.org/10.5306/wjco.v12.i4.217.
17. Cullis, J., Das, S. and Bar-Sagi, D. (2017). Kras and Tumor Immunity: Friend or Foe? *Cold Spring Harbor Perspectives in Medicine*, 8(9), p.a031849. doi:https://doi.org/10.1101/cshperspect.a031849.
18. Curran- NK cells
19. de Freitas, R.M. and da Costa Maranduba, C.M. (2015). Myeloproliferative neoplasms and the JAK/STAT signaling pathway: an overview. *Revista Brasileira de Hematologia e Hemoterapia*, 37(5), pp.348–353. doi:https://doi.org/10.1016/j.bjhh.2014.10.001.
20. de Haas, N., de Koning, C., Spilgies, L., de Vries, I.J.M. and Hato, S.V. (2016). Improving cancer immunotherapy by targeting the STATe of MDSCs. *OncoImmunology*, 5(7), p.e1196312. doi:https://doi.org/10.1080/2162402x.2016.1196312.
21. de Langen, A.J., Johnson, M.L., Mazieres, J., Dingemans, A.-M.C., Mountzios, G., Pless, M., Wolf, J., Schuler, M., Lena, H., Skoulidis, F., Yoneshima, Y., Kim, S.-W., Linardou, H., Novello, S., van der Wekken, A.J., Chen, Y., Peters, S., Felip, E., Solomon, B.J. and Ramalingam, S.S. (2023). Sotorasib versus docetaxel for previously treated non-small-cell lung cancer with KRASG12C mutation: a randomised, open-label, phase 3 trial. *The Lancet*. doi:https://doi.org/10.1016/s0140-6736(23)00221-0.
22. Denk, D. and Greten, F.R. (2022). Inflammation: the incubator of the tumor microenvironment. *Trends in Cancer*, 8(11), pp.901–914. doi:https://doi.org/10.1016/j.trecan.2022.07.002.

23. Elli, E.M., Baratè, C., Mendicino, F., Palandri, F. and Palumbo, G.A. (2019). Mechanisms Underlying the Anti-inflammatory and Immunosuppressive Activity of Ruxolitinib. *Frontiers in Oncology*, 9. doi:https://doi.org/10.3389/fonc.2019.01186.
24. Friedlaender, A., Drilon, A., Weiss, G.J., Banna, G.L. and Addeo, A. (2020). KRAS as a druggable target in NSCLC: Rising like a phoenix after decades of development failures. *Cancer Treatment Reviews*, 85, p.101978. doi:https://doi.org/10.1016/j.ctrv.2020.101978.
25. Gandini, S., Botteri, E., Iodice, S., Boniol, M., Lowenfels, A.B., Maisonneuve, P. and Boyle, P. (2007). Tobacco smoking and cancer: A meta-analysis. *International Journal of Cancer*, [online] 122(1), pp.155–164. doi:https://doi.org/10.1002/ijc.23033.
26. Garon, E.B., Chih-Hsin Yang, J. and Dubinett, S.M. (2020). The Role of Interleukin 1β in the Pathogenesis of Lung Cancer. *JTO Clinical and Research Reports*, 1(1), p.100001. doi:https://doi.org/10.1016/j.jtocrr.2020.100001.
27. Gomes, M., Teixeira, A.L., Coelho, A., Araújo, A. and Medeiros, R. (2014). The Role of Inflammation in Lung Cancer. *Advances in Experimental Medicine and Biology*, pp.1–23. doi:https://doi.org/10.1007/978-3-0348-0837-8_1.
28. Golay, H.G. and Barbie, D.A. (2014). Targeting cytokine networks in KRAS-driven tumorigenesis. *Expert Review of Anticancer Therapy*, 14(8), pp.869–871. doi:https://doi.org/10.1586/14737140.2014.928596.
29. Hamarsheh, S., Groß, O., Brummer, T. and Zeiser, R. (2020). Immune modulatory effects of oncogenic KRAS in cancer. *Nature Communications*, [online] 11(1), p.5439. doi:https://doi.org/10.1038/s41467-020-19288-6.
30. Hasan, G.M., Hassan, M.I., Sohal, S.S., Shamsi, A. and Alam, M. (2023). Therapeutic Targeting of Regulated Signaling Pathways of Non-Small Cell Lung Carcinoma. *ACS omega*, [online] 8(30), pp.26685–26698. doi:https://doi.org/10.1021/acsomega.3c02424.
31. Hu, X., li, J., Fu, M., Zhao, X. and Wang, W. (2021). The JAK/STAT signaling pathway: from bench to clinic. *Signal Transduction and Targeted Therapy*, 6(1). doi:https://doi.org/10.1038/s41392-021-00791-1.
32. Hu, Q., Bian, Q., Rong, D., Lin Feng Wang, Song, J., Huang, H.-S., Zeng, J., Mei, J. and Wang, P.-Y. (2023). JAK/STAT pathway: Extracellular signals, diseases, immunity, and therapeutic regimens. [online] 11. doi:https://doi.org/10.3389/fbioe.2023.1110765.
33. Huang, L., Guo, Z., Wang, F. and Fu, L. (2021). KRAS mutation: from undruggable to druggable in cancer. *Signal Transduction and Targeted Therapy*, [online] 6(1). doi:https://doi.org/10.1038/s41392-021-00780-4.
34. Huang, B., Lang, X. and Li, X. (2022). The role of IL-6/JAK2/STAT3 signaling pathway in cancers. *Frontiers in Oncology*, 12. doi:https://doi.org/10.3389/fonc.2022.1023177.
35. Jorgovanovic, D., Song, M., Wang, L. and Zhang, Y. (2020). Roles of IFN-γ in tumor progression and regression: a review. *Biomarker Research*, 8(1). doi:https://doi.org/10.1186/s40364-020-00228-x.
36. Karim, M.R., Hossain, D., Uddin, A.M. and Rume, F.I. (2022). *Chapter 7 - Role of macrophages in tumor development*. [online] ScienceDirect. Available at: https://www.sciencedirect.com/science/article/abs/pii/B9780128223680000074 [Accessed 20 Jan. 2024].

37. Kersten, K., de Visser, K.E., van Miltenburg, M.H. and Jonkers, J. (2016). Genetically engineered mouse models in oncology research and cancer medicine. *EMBO Molecular Medicine*, [online] 9(2), pp.137–153. doi:https://doi.org/10.15252/emmm.201606857.
38. Kim, D.M., Kim, M.J., Moon, J.-H., Lee, E.Y., Hong, J.K., Lee, S., Koh, D.-I., Ryu, Y.S., Kim, S.M., Jung, Soo-A., Shin, J.-S., Kim, J., Park, Y.S., Hong, S.-W., Lee, S.H., Jung, J., Park, S.S., Kim, D.Y., Kim, E.H. and Jeong, H.-R. (2020). Inhibition of JAK1/2 can overcome EGFR-TKI resistance in human NSCLC. *Biochemical and Biophysical Research Communications*, [online] 527(1), pp.305–310. doi:https://doi.org/10.1016/j.bbrc.2020.04.095.
39. Kirito, K. (2022). Recent progress of JAK inhibitors for hematological disorders. *Immunological Medicine*, pp.1–12. doi:https://doi.org/10.1080/25785826.2022.2139317.
40. Kitajima, S., Thummalapalli, R. and Barbie, D.A. (2016). Inflammation as a driver and vulnerability of KRAS mediated oncogenesis. *Seminars in Cell & Developmental Biology*, 58, pp.127–135. doi:https://doi.org/10.1016/j.semcdb.2016.06.009.
41. Klein, K., Stoiber, D., Sexl, V. and Witalisz-Siepracka, A. (2021). Untwining Anti-Tumor and Immunosuppressive Effects of JAK Inhibitors—A Strategy for Hematological Malignancies? *Cancers*, 13(11), p.2611. doi:https://doi.org/10.3390/cancers13112611.
42. Koukis, I., Gkiozos, I., Ntanos, I., Kainis, E. and Syrigos, K.N. (2013). Clinical and Surgical-Pathological Staging in Early Non-Small Cell Lung Cancer. *Oncology Reviews*, [online] 7(1). doi:https://doi.org/10.4081/oncol.2013.e7.
43. Liu, J.-F., Deng, W., Chen, L., Li, Y., Wu, L., Ma, S., Zhang, W., Bu, L. and Sun, Z. (2018). Inhibition of JAK2/STAT3 reduces tumor-induced angiogenesis and myeloid-derived suppressor cells in head and neck cancer. *Molecular Carcinogenesis*, 57(3), pp.429–439. doi:https://doi.org/10.1002/mc.22767.
44. Majoros, A., Platanitis, E., Kernbauer-Hölzl, E., Rosebrock, F., Müller, M. and Decker, T. (2017). Canonical and Non-Canonical Aspects of JAK–STAT Signaling: Lessons from Interferons for Cytokine Responses. *Frontiers in Immunology*, 8. doi:https://doi.org/10.3389/fimmu.2017.00029.
45. Marabese, M., Ganzinelli, M., Garassino, M.C., Shepherd, F.A., Piva, S., Caiola, E., Macerelli, M., Bettini, A., Lauricella, C., Floriani, I., Farina, G., Longo, F., Bonomi, L., Fabbri, M.A., Veronese, S., Marsoni, S., Broggini, M. and Rulli, E. (2015). *KRAS* mutations affect prognosis of non-small-cell lung cancer patients treated with first-line platinum containing chemotherapy. *Oncotarget*, [online] 6(32). doi:https://doi.org/10.18632/oncotarget.5607.
46. Mausey, N. and Halford, Z. (2023). Targeted Therapies for Previously 'Undruggable' KRAS-Mutated Non–Small Cell Lung Cancer: A Review of Sotorasib and Adagrasib. *Annals of Pharmacotherapy*. doi:https://doi.org/10.1177/10600280231197459.
47. Mellema, W.W., Dingemans, A.C., Thunnissen, E., Peter J.F. Snijders, Derks, J.L., Daniëlle A.M. Heideman, Robert-Jan van Suylen and Smit, E.F. (2013). KRAS Mutations in Advanced Nonsquamous Non–Small-Cell Lung Cancer Patients Treated with First-Line Platinum-Based Chemotherapy Have No Predictive Value. *Journal of Thoracic Oncology*, 8(9), pp.1190–1195. doi:https://doi.org/10.1097/jto.0b013e318298764e.

48. Mojic, M., Takeda, K. and Hayakawa, Y. (2017). The Dark Side of IFN-γ: Its Role in Promoting Cancer Immunoevasion. *International Journal of Molecular Sciences*, [online] 19(1), p.89. doi:https://doi.org/10.3390/ijms19010089.
49. Molina, J.R., Yang, P., Cassivi, S.D., Schild, S.E. and Adjei, A.A. (2008). Non-small Cell Lung cancer: epidemiology, Risk factors, treatment, and Survivorship. *Mayo Clinic Proceedings*, 83(5), pp.584–94. doi:https://doi.org/10.4065/83.5.584.
50. Mohrherr, J., Haber, M., Breitenecker, K., Aigner, P., Moritsch, S., Voronin, V., Eferl, R., Moriggl, R., Stoiber, D., Győrffy, B., Brcic, L., László, V., Döme, B., Moldvay, J., Dezső, K., Bilban, M., Popper, H., Moll, H.P. and Casanova, E. (2019). JAK-STAT inhibition impairs K-RAS-driven lung adenocarcinoma progression. *International Journal of Cancer*, [online] 145(12), pp.3376–3388. doi:https://doi.org/10.1002/ijc.32624.
51. Mugarza, E., van Maldegem, F., Boumelha, J., Moore, C., Rana, S., Llorian Sopena, M., East, P., Ambler, R., Anastasiou, P., Romero-Clavijo, P., Valand, K., Cole, M., Molina-Arcas, M. and Downward, J. (2022). Therapeutic KRAS ^{G12C} inhibition drives effective interferon-mediated antitumor immunity in immunogenic lung cancers. *Science Advances*, 8(29). doi:https://doi.org/10.1126/sciadv.abm8780.
52. Nicolas, C.S., Peineau, S., Amici, M., Csaba, Z., Fafouri, A., Javalet, C., Collett, V.J., Hildebrandt, L., Seaton, G., Choi, S.-L., Sim, S.-E., Bradley, C., Lee, K., Zhuo, M., Kaang, B.-K., Gressens, P., Dournaud, P., Fitzjohn, S.M., Bortolotto, Z.A. and Cho, K. (2012). The JAK/STAT Pathway Is Involved in Synaptic Plasticity. *Neuron*, [online] 73(2), pp.374–390. doi:https://doi.org/10.1016/j.neuron.2011.11.024.
53. Nooreldeen, R. and Bach, H. (2021). Current and Future Development in Lung Cancer Diagnosis. *International Journal of Molecular Sciences*, [online] 22(16), p.8661. doi:https://doi.org/10.3390/ijms22168661.
54. O'Shea, J.J., Schwartz, D.M., Villarino, A.V., Gadina, M., McInnes, I.B. and Laurence, A. (2015). The JAK-STAT Pathway: Impact on Human Disease and Therapeutic Intervention. *Annual Review of Medicine*, [online] 66(1), pp.311–328. doi:https://doi.org/10.1146/annurev-med-051113-024537.
55. Okita, R., Shimizu, K., Nojima, Y., Shinsuke Saisho and Nakata, M. (2019). JAK-STAT inhibitor overcomes interferon γ-reduced, NK cell-mediated cytotoxicity in non-small-cell lung cancer cells. *Annals of Oncology*, 30, pp.v800–v801. doi:https://doi.org/10.1093/annonc/mdz269.011.
56. Passaro, A., Mok, T., Peters, S., Popat, S., Ahn, M.-J. and de Marinis, F. (2021). Recent Advances on the Role of EGFR Tyrosine Kinase Inhibitors in the Management of NSCLC With Uncommon, Non Exon 20 Insertions, EGFR Mutations. *Journal of Thoracic Oncology*, 16(5), pp.764–773. doi:https://doi.org/10.1016/j.jtho.2020.12.002.
57. Pereira, F., Ferreira, A., Reis, C.A., Sousa, M.J., Oliveira, M.J. and Preto, A. (2022). KRAS as a Modulator of the Inflammatory Tumor Microenvironment: Therapeutic Implications. *Cells*, 11(3), p.398. doi:https://doi.org/10.3390/cells11030398.
58. Pfaffl, M.W. (2001). A new mathematical model for relative quantification in real-time RT–PCR. *Nucleic Acids Research*, [online] 29(9), p.e45. Available at: https://www.ncbi.nlm.nih.gov/pmc/articles/PMC55695/.
59. Román, M., Baraibar, I., López, I., Nadal, E., Rolfo, C., Vicent, S. and Gil-Bazo, I. (2018). KRAS oncogene in non-small cell lung cancer: clinical perspectives on the treatment of an old target. *Molecular Cancer*, [online] 17(1). doi:https://doi.org/10.1186/s12943-018-0789-x.

60. Ryan, M.B., Fece de la Cruz, F., Phat, S., Myers, D.T., Wong, E., Shahzade, H.A., Hong, C.B. and Corcoran, R.B. (2019). Vertical Pathway Inhibition Overcomes Adaptive Feedback Resistance to KRASG12C Inhibition. *Clinical Cancer Research*, 26(7), pp.1633–1643. doi:https://doi.org/10.1158/1078-0432.ccr-19-3523.
61. Sant, M., Daidone, C., Kaire Innos, Marcos-Gragera, R., Katrijn Vanschoenbeek, Miguel Rodriguez Barranco, Ester Oliva Poch and Lillini, R. (2023). Patterns of care and survival for lung cancer: Results of the European population-based high-resolution study. *Frontiers in epidemiology*, 3. doi:https://doi.org/10.3389/fepid.2023.1109853.
62. Schönberg, K., Rudolph, J., Vonnahme, M., Sowmya Parampalli Yajnanarayana, Cornez, I., Hejazi, M., Manser, A.R., Uhrberg, M., Verbeek, W., Steffen Koschmieder, Brümmendorf, T.H., Brossart, P., Heine, A. and Wolf, D. (2015). JAK Inhibition Impairs NK Cell Function in Myeloproliferative Neoplasms. *Cancer Research*, 75(11), pp.2187–2199. doi:https://doi.org/10.1158/0008-5472.can-14-3198.
63. Shim, H.S., Choi, Y.-L., Kim, L., Chang, S., Kim, W.-S., Roh, M.S., Kim, T.-J., Ha, S.Y., Chung, J.-H., Jang, S.J. and Lee, G.K. (2017). Molecular Testing of Lung Cancers. *Journal of Pathology and Translational Medicine*, [online] 51(3), pp.242–254. doi:https://doi.org/10.4132/jptm.2017.04.10.
64. Sung, H., Ferlay, J., Siegel, R.L., Laversanne, M., Soerjomataram, I., Jemal, A. and Bray, F. (2021). Global Cancer Statistics 2020: GLOBOCAN Estimates of Incidence and Mortality Worldwide for 36 Cancers in 185 Countries. *CA: a Cancer Journal for Clinicians*, 71(3), pp.209–249.
65. Taverna, J.A., Hung, C.-N., DeArmond, D.T., Chun Liang Chen, Huang, H.C., Osmulski, P.A., Gaczynska, M., Wang, C.-M., Lucio, N.D., Chih Wei Chou, Nazarullah, A., Lampkin, S.R., Qiu, L., Bearss, D.J., Warner, S.L., Whatcott, C.J., Mouritsen, L., Wade, M., Weitman, S.D. and Mesa, R.A. (2020). Single-Cell Proteomic Profiling Identifies Combined AXL and JAK1 Inhibition as a Novel Therapeutic Strategy for Lung Cancer. 80(7), pp.1551–1563. doi:https://doi.org/10.1158/0008-5472.can-19-3183.
66. Tan, S.-H. . and Nevalainen, M.T. (2008). Signal transducer and activator of transcription 5A/B in prostate and breast cancers. *Endocrine Related Cancer*, 15(2), pp.367–390. doi:https://doi.org/10.1677/erc-08-0013.
67. Tan, Z., Xue, H., Sun, Y., Zhang, C., Song, Y. and Qi, Y. (2021). The Role of Tumor Inflammatory Microenvironment in Lung Cancer. *Frontiers in Pharmacology*, 12. doi:https://doi.org/10.3389/fphar.2021.688625.
68. Taylor, P.C., Laedermann, C., Alten, R., Feist, E., Choy, E., Haladyj, E., De La Torre, I., Richette, P., Finckh, A. and Tanaka, Y. (2023). A JAK Inhibitor for Treatment of Rheumatoid Arthritis: The Baricitinib Experience. *Journal of Clinical Medicine*, [online] 12(13), p.4527. doi:https://doi.org/10.3390/jcm12134527.
69. Tzeng, H.-T., I-Tsu Chyuan and Lai, J.-H. (2021). Targeting the JAK-STAT pathway in autoimmune diseases and cancers: A focus on molecular mechanisms and therapeutic potential. 193, pp.114760–114760. doi:https://doi.org/10.1016/j.bcp.2021.114760.
70. Velcich, A., Klampfer, L., Mariadason, J., Smartt, H., Guilmeau, S., Maier, S., Yang, W., Christman, J., Heerdt, B. and Augenlicht, L. (2006). *CHAPTER 3 - Genetics and Epigenetics in Cancer Biology*. [online] ScienceDirect. Available at: https://www.sciencedirect.com/science/article/pii/B9780120883936500592 [Accessed 19 Jan. 2024].
71. Wistuba, I.I., Brambilla, E. and Noguchi, M. (2018). *17 - Classic Anatomic Pathology and Lung Cancer*. [online] ScienceDirect. Available at:

https://www.sciencedirect.com/science/article/abs/pii/B9780323523578000172 [Accessed 18 Jan. 2024].
72. Witalisz-Siepracka, A., Klein, K., Prinz, D., Leidenfrost, N., Schabbauer, G., Dohnal, A. and Sexl, V. (2019). Loss of JAK1 Drives Innate Immune Deficiency. *Frontiers in Immunology*, 9. doi:https://doi.org/10.3389/fimmu.2018.03108.
73. Xie, M., Zheng, H., Madan-Lala, R., Dai, W., Gimbrone, N.T., Chen, Z., Kinose, F., Blackstone, S.A., Smalley, K.S.M., Cress, W.D., Haura, E.B., Rix, U. and Beg, A.A. (2019). MEK Inhibition Modulates Cytokine Response to Mediate Therapeutic Efficacy in Lung Cancer. *Cancer Research*, [online] 79(22), pp.5812–5825. doi:https://doi.org/10.1158/0008-5472.can-19-0698.
74. Zhou, J.X., Yang, H., Deng, Q., Gu, X., He, P., Lin, Y., Zhao, M., Jiang, J., Chen, H., Lin, Y., Yin, W., Mo, L. and He, J. (2013). Oncogenic driver mutations in patients with non-small-cell lung cancer at various clinical stages. *Annals of Oncology*, [online] 24(5), pp.1319–1325. doi:https://doi.org/10.1093/annonc/mds626.
75. Zhu, G., Pei, L., Xia, H., Tang, Q. and Bi, F. (2021). Role of oncogenic KRAS in the prognosis, diagnosis and treatment of colorectal cancer. *Molecular Cancer*, 20(1). doi:https://doi.org/10.1186/s12943-021-01441-4.
76. Zhang, X., Zeng, Y., Qu, Q., Zhu, J., Liu, Z., Ning, W., Zeng, H., Zhang, N., Du, W., Chen, C. and Huang, J.-A. (2017). PD-L1 induced by IFN-γ from tumor-associated macrophages via the JAK/STAT3 and PI3K/AKT signaling pathways promoted progression of lung cancer. *International Journal of Clinical Oncology*, [online] 22(6), pp.1026–1033. doi:https://doi.org/10.1007/s10147-017-1161-7.
77. Zhang, J. and Veeramachaneni, N. (2022). Targeting interleukin-1β and inflammation in lung cancer. *Biomarker Research*, 10(1). doi:https://doi.org/10.1186/s40364-021-00341-5.
78. Zeissig, M.N., Ashwood, L.M., Kondrashova, O. and Sutherland, K.D. (2023). Next batter up! Targeting cancers with KRAS-G12D mutations. *Trends in Cancer*. doi:https://doi.org/10.1016/j.trecan.2023.07.010.
79. Zito Marino, F., Bianco, R., Accardo, M., Ronchi, A., Cozzolino, I., Morgillo, F., Rossi, G. and Franco, R. (2019). Molecular heterogeneity in lung cancer: from mechanisms of origin to clinical implications. *International Journal of Medical Sciences*, [online] 16(7), pp.981–989. doi:https://doi.org/10.7150/ijms.34739.

List of Figures

List of Tables